

Monsoon sensitivity to aerosol direct radiative forcing in the community atmosphere model

S SAJANI^{1,*}, K KRISHNA MOORTHY², K RAJENDRAN¹ and RAVI S NANJUNDIAH^{3,4}

¹*CSIR-Centre for Mathematical Modelling and Computer Simulation, Bangalore 560 037, India.*

²*Space Physics Laboratory, Vikram Sarabhai Space Centre, Thiruvananthapuram, India.*

³*Centre for Atmospheric and Oceanic Sciences, Indian Institute of Science, Bangalore 560 012, India.*

⁴*Divecha Centre for Climate Change, Indian Institute of Science, Bangalore 560 012, India.*

*Corresponding author. e-mail: sajanirajendran@gmail.com

Aerosol forcing remains a dominant uncertainty in climate studies. The impact of aerosol direct radiative forcing on Indian monsoon is extremely complex and is strongly dependent on the model, aerosol distribution and characteristics specified in the model, modelling strategy employed as well as on spatial and temporal scales. The present study investigates (i) the aerosol direct radiative forcing impact on mean Indian summer monsoon when a combination of quasi-realistic mean annual cycles of scattering and absorbing aerosols derived from an aerosol transport model constrained with satellite observed Aerosol Optical Depth (AOD) is prescribed, (ii) the dominant feedback mechanism behind the simulated impact of all-aerosol direct radiative forcing on monsoon and (iii) the relative impacts of absorbing and scattering aerosols on mean Indian summer monsoon. We have used CAM3, an atmospheric GCM (AGCM) that has a comprehensive treatment of the aerosol–radiation interaction. This AGCM has been used to perform climate simulations with three different representations of aerosol direct radiative forcing due to the total, scattering aerosols and black carbon aerosols. We have also conducted experiments without any aerosol forcing. Aerosol direct impact due to scattering aerosols causes significant reduction in summer monsoon precipitation over India with a tendency for southward shift of Tropical Convergence Zones (TCZs) over the Indian region. Aerosol forcing reduces surface solar absorption over the primary rain-belt region of India and reduces the surface and lower tropospheric temperatures. Concurrent warming of the lower atmosphere over the warm oceanic region in the south reduces the land–ocean temperature contrast and weakens the monsoon overturning circulation and the advection of moisture into the land-mass. This increases atmospheric convective stability, and decreases convection, clouds, precipitation and associated latent heat release. Our analysis reveals a defining negative moisture-advection feedback that acts as an internal damping mechanism spinning down the regional hydrological cycle and leading to significant circulation changes in response to external radiative forcing perturbations. When total aerosol loading (both absorbing and scattering aerosols) is prescribed, dust and black carbon aerosols are found to cause significant atmospheric heating over the monsoon region but the aerosol-induced weakening of meridional lower tropospheric temperature gradient (leading to weaker summer monsoon rainfall) more than offsets the increase in summer-time rainfall resulting from the atmospheric heating effect of absorbing aerosols, leading to a net decrease of summer monsoon rainfall. Further, we have carried out climate simulations with globally constant AODs and also with the constant AODs over the extended Indian region replaced by realistic AODs. Regional aerosol radiative forcing perturbations over the Indian region is found to have impact not only over the region of loading but over remote tropical regions as well. This warrants the need to prescribe realistic aerosol properties in strategic regions such as India in order to accurately assess the aerosol impact.

Keywords. Monsoon; aerosol direct radiative forcing; moisture-advection feedback.

1. Introduction

In recent times, the importance of atmospheric aerosols, both natural and anthropogenic, in radiative forcing, hydrological cycle and atmospheric chemistry with implications to global climate is being increasingly realised. The aerosols affect climate directly by reflecting and absorbing solar radiation, and to a lesser extent through absorption and emission of longwave radiation. Absorbing aerosols such as dust and black carbon (BC) are characterized by their ability to heat the atmosphere by absorbing solar radiation. In contrast, non-absorbing aerosols such as sulphate scatter solar radiation and have relatively weak atmospheric heating effect. Yet, both absorbing and non-absorbing aerosols cause surface cooling by blocking solar radiation from reaching the earth surface, referred to as aerosol solar dimming effect (which can partly be contributed by long term changes in clouds). They also affect the climate indirectly by altering the amount and size of cloud condensation nuclei in the atmosphere. The chemical composition and size distribution of aerosols effectively characterize their optical properties. The physical properties of aerosols are also strong functions of their sources, which are widely distributed and highly variable from one region to the other. Thus, the aerosol impact on climate system has a strong regional component. The variety of aerosol sources (natural and anthropogenic), the wide size spectrum and their lifetimes result in a spatially and temporally heterogeneous aerosol field, making aerosol characterization in climate models, a real challenge. Hence, much uncertainty is attributed to the role of aerosols on climate.

Summer monsoon over India is largely controlled by the internal and external forcings such as sea surface temperature (SST), Tibetan Plateau heating, soil moisture, Eurasian snow cover, greenhouse gas concentration, and aerosols. Among them, the effect of aerosols over India, where the emission of aerosol precursors has been rapidly increasing during the last decades and is expected to continue to increase for the coming decades as a result of the economic development of the region (Streets and Waldhoff 2000), can be a significantly influential factor. In Asian monsoon regions, the aerosol dimming effect is especially large due to heavy pollution, and frequent occurrence of dust storms.

Several studies have analyzed the impact of aerosols on climate. Mitchell *et al.* (1995) using the Hadley Centre atmospheric General Circulation Model (GCM) coupled to a mixed layer ocean and Haywood *et al.* (1997) using the Hadley Centre atmospheric GCM found that the agreement between models and observation is improved in climate simulations if tropospheric sulphate

aerosols are included. Roeckner *et al.* (1999) using ECHAM4 coupled GCM found that the intensity of the global hydrological cycle becomes weaker if direct and indirect sulphate aerosol effects are included. Atmospheric and coupled ocean-atmospheric GCMs have been used with quasi-realistic aerosol specifications to examine the effect of aerosols on the mean Indian monsoon. Ramanathan *et al.* (2005) using NCAR PCM coupled GCM with sulphate aerosol and Atmospheric Brown Cloud Radiative Forcing showed that as a result of global dimming, the Indian monsoon is reduced on decadal or longer time scales. Many studies have also analyzed the impact of absorbing aerosols on climate. Chung *et al.* (2002) using the NCAR CCM3 GCM (to study January–March period) and Menon *et al.* (2002) using a time invariant aerosol radiative forcing showed that absorbing aerosols lead to enhanced low-level convergence and precipitation over the haze area including India and China. Chakraborty *et al.* (2004) using prescribed aerosol direct radiative forcing in the NCMRWF GCM (a modified version of NCEP model) found that the local warming impact of absorbing aerosols leads to an overall increase in pre-monsoon rainfall over Indian region. However, during monsoon season, the precipitation changes in the continental region are found to be highly sensitive to the parameterization of deep convection in the model. Lau *et al.* (2006) pointed out that, on intraseasonal to interannual time scales, heating by absorbing aerosols induces a tropospheric temperature anomaly over northern India and Tibetan regions in late spring and early summer, subsequently leading to an earlier onset and intensification of the Indian monsoon in June–July. They suggest that the ‘elevated heat pump’ effect of atmospheric heating by dust transported from the nearby deserts to northern India, stacking up against the southern slopes of the Himalayas has an important effect on monsoons. The dust combined with BC from industrial and agricultural pollution in northern India provide an anomalous diabatic heat source, which triggers positive feedback in monsoon convective heating, enhancing the Indian monsoon.

In an observational study, Bollasina *et al.* (2008) found that in years when more aerosols are observed in May, cloud and precipitation amounts are reduced, increasing the surface temperature through solar heating. This results in a stronger June/July monsoon. In a comprehensive study, Meehl *et al.* (2008) using global seasonally varying BC aerosol distributions in NCAR CCSM coupled GCM, showed that the BC aerosols act to increase meridional tropospheric temperature gradient in the pre-monsoon months of March–April–May, particularly between the elevated heat source

of the Tibetan Plateau and areas to the south and contribute to enhanced precipitation over India in those months. But, with the onset of the monsoon, the reduced surface temperatures in the Bay of Bengal, Arabian Sea, and over India that extend to the Himalayas act to reduce monsoon rainfall over India itself, with some small increases over the Tibetan Plateau. Wang *et al.* (2009) studied the impact of aerosols simulated by an aerosol chemistry transport model (without assimilation of realistic aerosol property to constrain the simulations) and found that the absorbing aerosols have dominant impact in intensifying the monsoon rainfall. But, the prescribed absorbing aerosols that contains external black carbon (BC) and the mixture of BC and sulphate, are too high compared to those used in other studies. Similarly the scattering aerosol run reflects the effect of solar absorption by sulphate and organic carbon because of their optical properties specified in the model. Further, the dominant impact is found to be over north and north-west of India despite the major rainbelt simulated by the control simulation of NCAR community atmospheric model is centered within 10–20°N). Collier and Zhang (2009) also studied the impact of aerosol radiative forcing on Indian summer monsoon but based on the simulation of one single monsoon season that is too short to derive meaningful climate statistics. Zhang *et al.* (2009) studied the effect of carbonaceous aerosols (containing both scattering and absorbing species) but with the focus on climate in east Asia. The dominant feedback mechanism behind the suppression of monsoon rainfall by a quasi-realistic aerosol forcing that is a mixture of both types of aerosols is not yet clearly brought out.

While the previous studies indicate plausible but different scenarios of aerosol impacts; they suggest that aerosol effects on monsoon water cycle dynamics are extremely complex, strongly dependent on aerosol distribution and characteristics specified in the climate model (e.g., loading, species, optical properties), climate model used (fidelity in simulating the mean monsoon, seasonal variation, etc.) and modelling strategy employed (coupled/stand-alone) as well as on spatial (regional/global) and temporal scales (monthly/seasonal/intraseasonal). Hence, aerosol forcing remains a dominant uncertainty (the level of scientific understanding ranging from low to medium, see IPCC 4th assessment report (Forster *et al.* 2007)) and its impact on monsoon is a challenging problem for climate variability.

In view of these important issues, we have carried out a set of climate integrations, to address the following objectives:

- What is the impact of aerosol direct radiative forcing on the mean monsoon when we prescribe

a quasi-realistic total aerosol forcing (combination of both scattering and absorbing aerosols) derived from an aerosol transport model and constrained with satellite observed Aerosol Optical Depth (AOD),

- What is the dominant feedback mechanism behind the simulated impact of aerosol direct radiative forcing, and
- What are the relative roles of absorbing and scattering aerosols on monsoon?

For this purpose, we have used an atmospheric GCM, NCAR Community Climate Model Version 3 (CAM3). This model incorporates a comprehensive treatment of the aerosol–radiation interaction. Its simulation of the seasonal mean monsoon rainfall is comparable to that of the other state-of-the-art GCMs.

We have conducted a set of four climate simulations, the first without any aerosol forcing (henceforth termed as the control simulation) and with three different representations of aerosol direct radiative forcing (i.e., total aerosols (10 species of sulphate, carbonaceous, dust and sea salt), scattering aerosols alone and black carbon (soot) alone). The aerosol climatologies were derived from the simulations with an aerosol transport model. In addition, we have carried out a constant global AOD simulation and a simulation where the constant AODs over the extended Indian region is prescribed from observation. The aim of the first of these two experiments was to get the climate sensitivity to a uniform aerosol forcing. With the second experiment, we have examined the climatic response to a substantial regional perturbation. All the integrations are of 10-year duration after spin-up and we have carried out a comprehensive analysis taking into account the climatological bias in the simulation of Indian summer monsoon by the control simulation. We examine the seasonal mean responses and neglect aerosol indirect effects and the effect of interactive SSTs. Section 2 describes the model, data and the set of simulations used in the study. Section 3 presents the aerosol direct radiative forcing based on the set of simulations. Section 4 analyses the impact of aerosol direct radiative forcing on Indian monsoon and dominant mechanism behind it. A brief summary and concluding remarks are given in section 5.

2. Model, data and simulations

2.1 Model

The atmospheric general circulation model used in this study is CAM3 of National Center for Atmospheric Research (NCAR), USA (Collins *et al.* 2006a, 2006b). In this study, CAM3 is integrated

Table 1. Definition of the four climate simulations used in the study.

Simulation	Aerosol specification	Duration
NO_AERO	NCAR CAM3 AGCM (T42L26) without any aerosol component in radiation scheme	10 years
BKG_AERO	Shortwave direct effect in the radiation scheme; scattering by background sulphate aerosols with uniform 0.15 AOD globally	10 years
ACE_AERO	Same as BKG_AERO, but AOD over Indian region (30°S – 35°N ; 30° – 110°E) is replaced with observation (ACE-Network observed AOD climatology integrated into MODIS climatology)	10 years
ALL_AERO	Shortwave direct effect of 10 aerosol species (4 types of dust, sulphate, sea salt, hydrophilic and hydrophobic black and organic carbons) is incorporated in the radiation scheme	10 years
BC_AERO	Shortwave direct effect of absorbing black carbon (1 type aerosol alone) is incorporated in the radiation scheme	10 years
SUL_AERO	Shortwave direct effect of scattering sulphate (1 type aerosol alone) is incorporated in the radiation scheme	10 years

with an interactive Community Land Model, a thermodynamic sea ice model but with SSTs prescribed from climatology. The version used in this study uses the Eulerian dynamical core at T42 spectral truncation, which is approximately $2.8^{\circ}\times 2.8^{\circ}$ on a Gaussian grid. The model uses a hybrid η -coordinate with 26 levels in the vertical. The parameterization of deep convection in CAM3 is based on the mass flux scheme of Zhang and McFarlane (1995), but with the addition that the convective cloud fraction is explicitly included.

The formulation of shortwave radiation follows δ -Eddington approximation of Joseph *et al.* (1976) and Coakley *et al.* (1983) and is described in detail in Briegleb (1992). The solar spectrum is divided into 19 discrete spectral and pseudo-spectral intervals (7 for O_3 , 1 for the visible, 7 for H_2O , 3 for CO_2 , and 1 for the near-infrared following Collins 1998). The CAM3 model atmosphere consists of a discrete vertical set of horizontally homogeneous layers within which radiative heating rates are to be specified. Each of these layers is considered to be a homogeneous combination of several radiatively active constituents. Solar irradiance, surface reflectivity for direct and diffuse radiation in each spectral interval, and the cosine of the solar zenith angle are specified. The surface albedo is specified in two wavebands (0.2–0.7 and 0.7–5.0 μm) and distinguishes albedos for direct and diffuse incident radiation. Albedos for ocean surfaces, geographically varying land surfaces, and sea ice surfaces are distinguished. The δ -Eddington scheme is implemented so that the solar radiation is evaluated once every model hour over the sunlit portions of the model earth.

2.2 Data and simulations

We have performed six CAM3 sensitivity simulations each of 10-year duration after spin-up for this study. In all the simulations, SST is prescribed using monthly climatological SST from HadISST data (Rayner *et al.* 2003). Table 1 lists the CAM3 simulations performed and analyzed in this study. The first 10-year simulation is the control run with no aerosol (henceforth referred to as ‘NO_AERO’) and the second is a 10-year integration of the model with a uniform background sulphate aerosol distribution of 0.15 AOD everywhere (hereafter referred to as ‘BKG_AERO’). The optics for background aerosol is identical to the sulphate aerosols described by Kiehl and Briegleb (1993). For precipitation validation, we have used CPC Merged Analysis of Precipitation (CMAP) on $2.5^{\circ}\times 2.5^{\circ}$ grid during 1979–2009 period (Xie and Arkin 1997).

2.2.1 AODs over India: Aerosol Climatology Effects (ACE) observations

India with its varied geographic features, distributed urbanization, extended coastal areas and dense population provides a unique scenario where regional scale aerosol variations could be important. But, there is a dearth of high resolution data pertaining to aerosol properties in India. To systematically study atmospheric aerosols, Aerosol Climatology and Effects (ACE) project was conceived under Indian Space Research Organization-Geosphere Biosphere Programme (ISRO-GBP). Under ACE programme, a well-maintained network of multiwavelength radiometers over selected

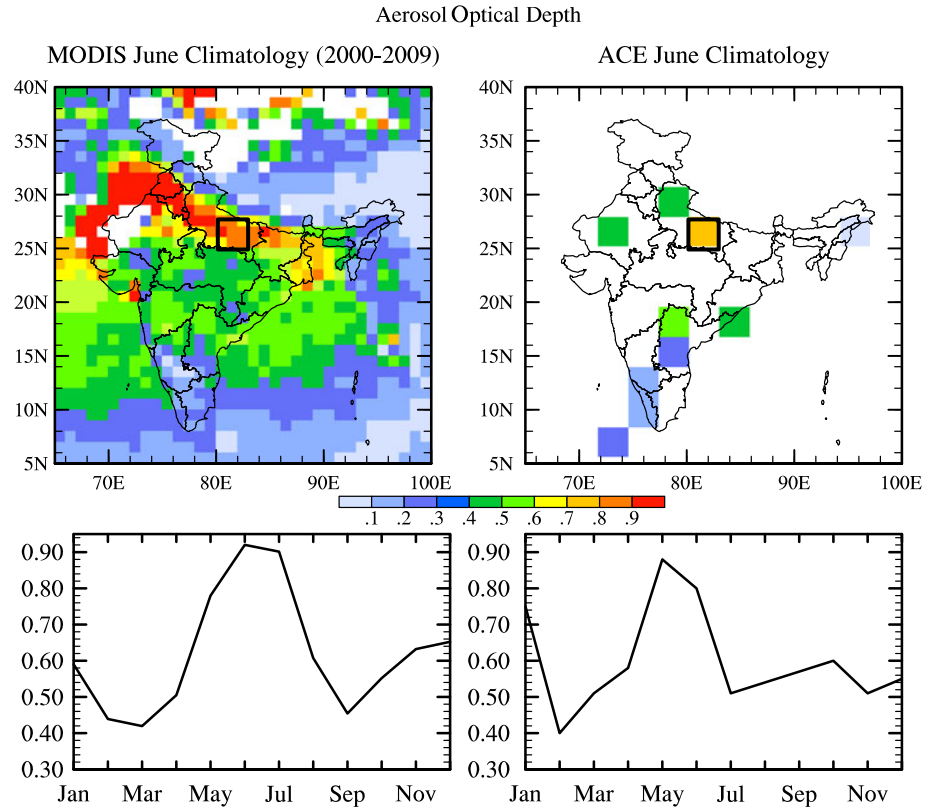


Figure 1. Climatological AOD for June from (a) MODIS (top left) and (b) ACE observations (top right). AOD mean annual cycle over a T42 grid at Kanpur (shown by square boxes in top panels) from (c) MODIS data (bottom left) and (d) ACE observation at Kanpur site (bottom right).

land sites in India provide spectrally resolved AODs over coastal, marine, arid, continental and urban environments. This network has been conceived to represent distinct aerosol environment owing to the influence of different source types and removal mechanisms. This activity provides continuous database with the ultimate objective of providing aerosol climatology for the Indian region (Moorthy *et al.* 1998). ACE climatological columnar AOD centered at 500 nm for June is compared with the corresponding AOD centered at 550 (545–565) nm from Moderate Resolution Imaging Spectroradiometer instrument (MODIS, Terra Level 3 global monthly data on $1^\circ \times 1^\circ$ grid retrieved from <http://modis.gsfc.nasa.gov/data/>) in figure 1. The AOD distribution from 10 stations over India, the mean annual cycle of AOD at a selected ACE network site, Kanpur (highlighted in a square grid) and a corresponding grid averaged AOD from MODIS data are also shown in figure 1. Clearly, there is large spatial heterogeneity of optical depth over India. In addition, there exists significant seasonal variation at a given grid as well. Overall, there is reasonable agreement between ACE and MODIS estimations for both spatial and temporal variability of AOD over India. However, there are slight differences between MODIS estimates

and ACE observations. These might be due to different spatial integrations of the two instruments. In addition, MODIS retrievals are ‘looking down’ while the ground instruments are always ‘looking up’ at the Sun. If the atmosphere is inhomogeneous, these can cause differences. Another possible reason for the difference could be that the MODIS AOD algorithms may be dependent on the satellite’s look-angle.

The third simulation (hereafter referred to as ‘ACE_AERO’) used in this study is similar to BKG_AERO, but realistic AOD is specified over the extended Indian region (30° – 110° E; 30° S– 35° N). For this, the AOD data over Indian region comprises 12-month climatological AOD (2000–2009 mean) computed from MODIS combined with climatological AOD from ACE observations available at 10 sites in India. We first replaced the MODIS data by ACE data over the land points where it is available and then regressed to the model grid. Background AOD of 0.15 is specified elsewhere.

2.2.2 Global aerosols

Fourth 10-year sensitivity simulation (henceforth referred to as ‘ALL_AERO’) uses four chemical

species of aerosol, viz., sea salt, soil dust, black and organic carbonaceous aerosols, and sulphate. The loadings of these aerosol types are prescribed from three-dimensional monthly distribution of these aerosols from output of the Model for Atmospheric Chemistry and Transport (MATCH, Rasch *et al.* 1997). The annually-cyclic tropospheric aerosol climatology consists of three-dimensional, monthly mean distributions of aerosol mass for:

- sulphate from natural and anthropogenic sources,
- sea salt,
- black and organic carbon derived from natural and anthropogenic sources, and
- soil dust.

There are four size categories of dust spanning diameters from 0.01 to 10 μm , and the black and organic carbon are represented by two tracers each for the hydrophobic (new) and hydrophilic (aged) components. The climatology therefore contains 10 types of aerosols, viz., sea salt, four size bins of soil dust, sulphate, new and aged BC, and hydrophobic and hydrophilic organic carbons. The prescribed aerosols include two species, the soil dust and carbonaceous types, which are strongly absorbing in visible wavelengths and hence increase the short-wave diabatic heating of the atmosphere. MATCH model is integrated using the National Centers for Environmental Prediction (NCEP) meteorological reanalysis (Kalnay *et al.* 1996). In MATCH model, each aerosol species, has a scale height varying from 1 km for large dust particle to 3.8 km for carbon. The aerosols are then interpolated to CAM3 vertical levels. For BKG_AERO and ACE_AERO, it is equally distributed in the lowest 3 km.

The three intrinsic optical properties stored for each of the 10 aerosol types are specific extinction, single scattering albedo, and asymmetry parameter from the Optical Properties of Aerosols and Clouds (OPAC) dataset (Hess *et al.* 1998). The aerosol types affected by hygroscopic growth are sulphate, sea salt, and hydrophilic organic carbon. The actual profiles of relative humidity computed from the model state in each radiation time step are used in the calculation. The optics for black and organic carbon is identical to the optics for soot and water-soluble aerosols in OPAC dataset. The bulk formulae of Cess (1985) are used to combine the optical properties of the individual aerosol species into a single set of bulk aerosol extinctions, single-scattering albedos, and asymmetry parameters for each layer.

Figure 2 shows mean annual cycles of AOD for total, carbon, dust and sulphate aerosols averaged over 70°N–100°E (which are prescribed in ALL_AERO). Annual cycle of total AOD shows

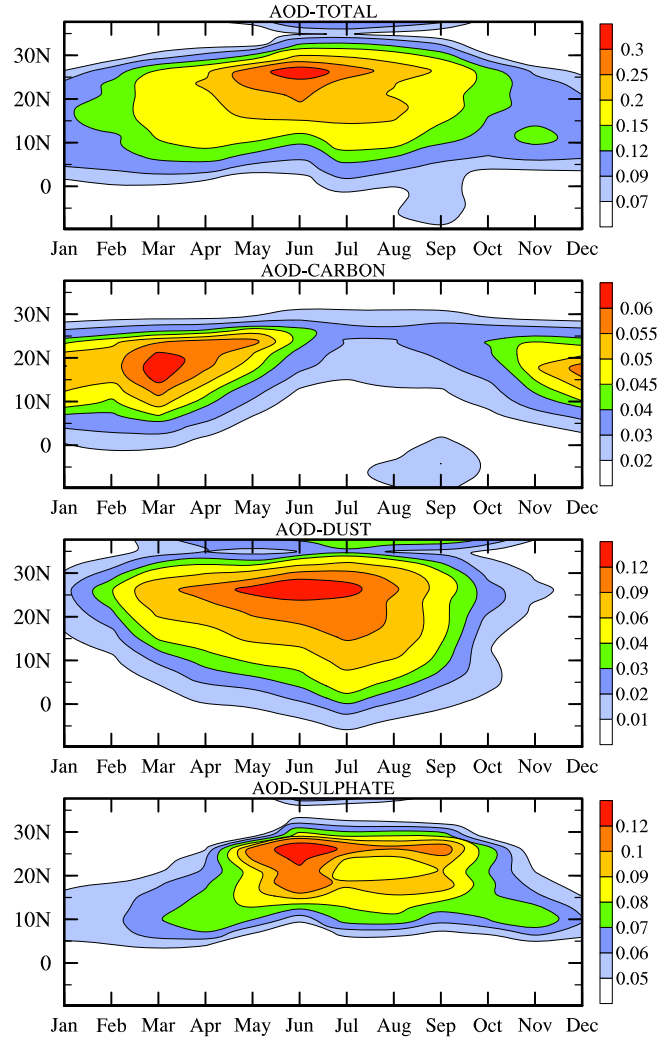


Figure 2. Mean annual cycle of AOD averaged over 70°–95°E for total, carbon, dust and sulphate aerosols from MATCH simulation.

high aerosol loadings over the Indian region during the pre-monsoon and monsoon months (February–September). There are distinct seasonal cycles in carbon and dust aerosols over India. The largest build-up of carbonaceous aerosol begins in November when the prevailing winds are northeasterlies, peaks in February–March and diminishes in June through September due to removal by the monsoon rain. This is consistent with the estimates of carbonaceous aerosols in Meehl *et al.* (2008). The strengthening of dust aerosols AOD in premonsoon season could be due to the prevailing low-level winds that transport them from desert regions into northwest of India. Sulphate aerosols show maximum build-up in premonsoon and monsoon seasons. All these combine to produce a strong seasonality in the total aerosol loading, rising rapidly in boreal spring (March–April–May), peaking in May before the start of the monsoon rainy season

over India, and declining during the summer monsoon and the following season as monsoon rainfall removes the aerosols. During monsoon months, the major contributions to total AOD over Indian region are from sulphate and dust aerosols. Of these two, dust is predominantly absorbing while sulphate is a scattering aerosol.

Figure 3 shows the climatological summer mean (June to August, JJAS) distribution of AOD of total aerosol and individual aerosol types (carbon, dust, sulphate and sea salt) over the Afro-Asian region. Total AOD is high over the monsoonal regions of Africa, and south and east Asia. The highest atmospheric loading of carbon occurs in east Asia, primarily over eastern part of China. Other areas with high loading of carbonaceous

aerosols include the Indian subcontinent and central Africa. Examining the distribution of carbon and sulphate aerosols we note that the pattern is closely associated with industrial activity over India and China. We also note that the distribution of AODs shows much higher concentration of carbon and sulphate aerosols over China *vis-a-vis* India. Over northern Africa and northwest India, AOD due to dust aerosols is very high. High values of AOD related to dust aerosols over northwest India could be due to transport of aerosols by prevailing winds during the summer season from deserts of Saudi Arabia and Africa. Sea salt concentrations are high over oceans with highest wind speed. Over the continental convective centres of ITCZ (Intertropical Convergence Zone) the major contribution to total aerosol appears to be from sulphate and dust aerosols. We also find that over the Indian region, the amount of sulphate aerosols are much larger than carbon and thus the contribution from non-absorbing (scattering) aerosols to total aerosol is comparable to or more than that of absorbing aerosols.

To study the relative roles of absorbing aerosols and scattering aerosols separately, we have carried out two 10-year simulations (after spin-up). The first simulation is with only black carbon (soot) which is the only purely absorbing aerosol (single scattering albedo close to zero in visible wavelengths, hereafter referred to as BC_AERO run). The second simulation is with only model generated sulphate aerosols which is purely scattering (i.e., single scattering albedo close to one in visible wavelengths at all humidity values, hereafter referred to as SUL_AERO).

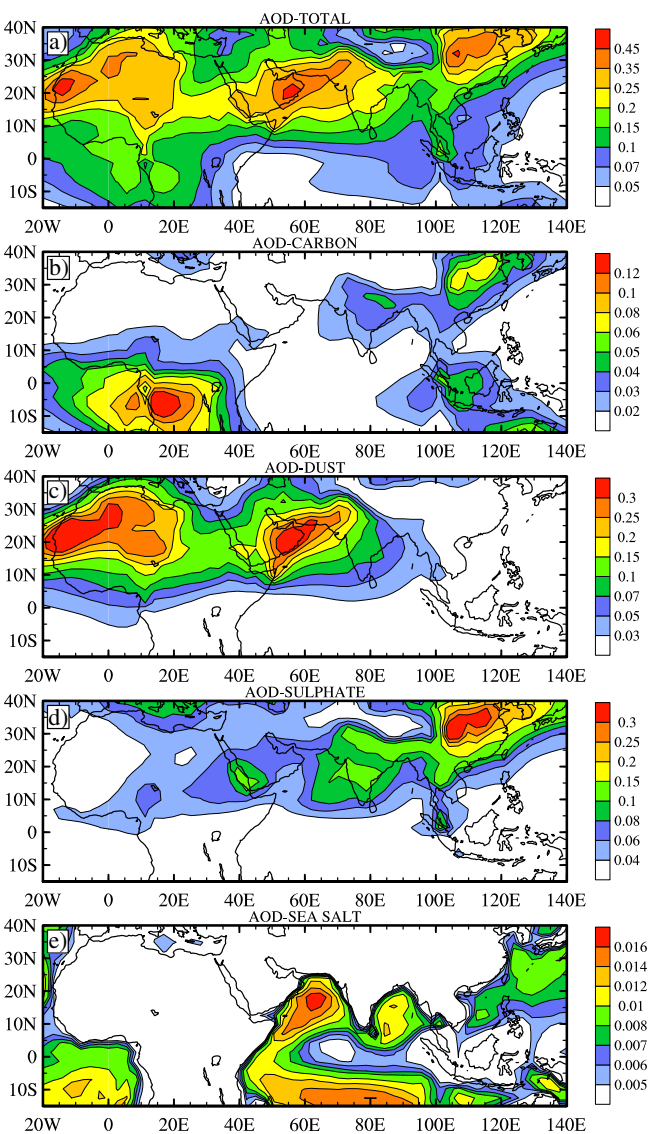


Figure 3. Climatological JJAS mean AOD of total, carbon, dust, sulphate and sea salt aerosols over the Afro-Asian region from MATCH simulation.

3. Aerosol direct radiative forcing

We first examine the perturbations caused by aerosols in the radiative forcing. Figure 4 shows the boreal summer (JJAS) aerosol solar radiative forcing averaged over Indian longitudes (70° – 95° E) from BKG_AERO, ACE_AERO, and ALL_AERO simulations (differences with respect to corresponding NO_AERO estimates). Similarly, figure 5 shows the distribution of corresponding aerosol-induced changes in JJAS mean total cloud amount. We examine the absorption of shortwave radiation by the atmosphere (F_{ATM}) in figure 4(a). While there is a warming *vis-a-vis* the control in the ALL_AERO simulation, the other two simulations (BKG_AERO and ACE_AERO) show cooling. The impact of aerosols is seen to be the highest over the northern parts of the subcontinent between 20° and 30° N – a region where the aerosol concentration is the highest. We discuss the changes in organized convection due to the effect of aerosols in section 4.

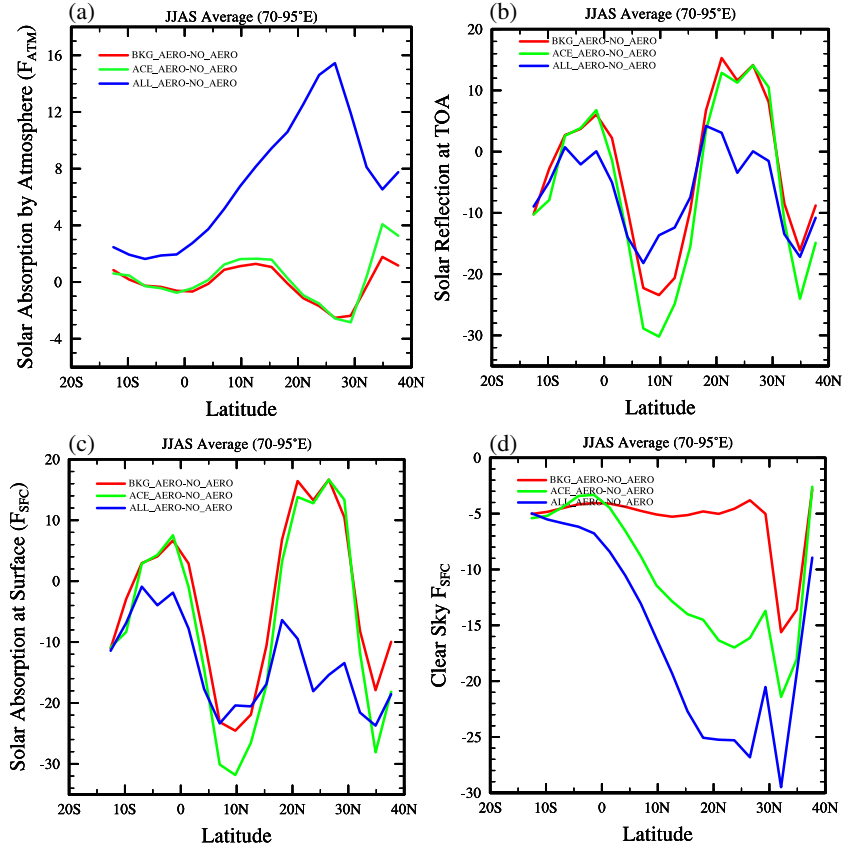


Figure 4. Simulated changes in JJAS mean aerosol solar radiative forcing (in Wm^{-2}) over India (70° – 95° E average) for BKG_AERO, ACE_AERO and ALL_AERO with respect to NO_AERO; (a) solar absorption by the atmosphere, (b) solar reflection at top of the atmosphere (TOA), (c) net solar absorption at the surface and (d) net solar absorption by the surface under clear sky condition.

Solar absorption by the atmosphere (F_{ATM} , figure 4a) shows that summer mean shortwave depletion by atmosphere peaks over northern continental region which is characterized by large changes in organized convection (section 4) and associated cloudiness (figure 5) in response to aerosol forcings. When absorbing aerosols are absent (for example in BKG_AERO and ACE_AERO), this depletion is much less (or opposite to that in ALL_AERO) and occurs mainly in response to scattering aerosols. F_{ATM} is reduced (becomes negative) over regions where there is large reduction in convection and cloud cover (figure 5). On the contrary, atmospheric absorption is increased over areas where scattering aerosols increase convection and cloud cover. Expectedly, in ALL_AERO in which absorbing species such as dust and carbonaceous aerosols are included, we notice considerable increase in atmospheric absorption over the entire monsoonal region. In ALL_AERO, atmospheric absorption by aerosols such as carbonaceous and dust particles is more dominant than that by clouds. We also note that the cloudiness is reduced over the continental monsoon region where aerosol concentration is the highest.

Summer mean solar reflection at TOA, F_{TOA} (figure 4b), is mainly controlled by nonabsorbing

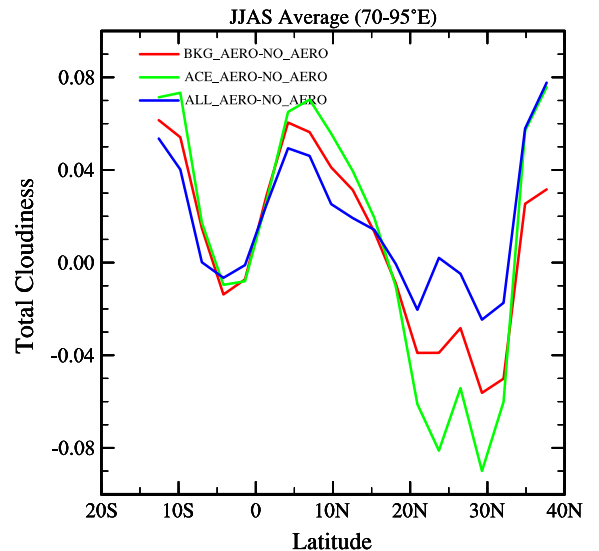


Figure 5. Simulated changes in JJAS mean total cloud amount (fraction) over India (70° – 95° E average) for BKG_AERO, ACE_AERO and ALL_AERO with respect to NO_AERO.

aerosols such as sulphates, and by cloud-radiation interaction. The distribution of the aerosol reflection differs from that of the absorption, but both aerosol absorption and reflection reduce downward solar insolation, so the net solar absorption by the surface (F_{SFC} , figure 4c) is reduced more than F_{TOA} (figure 4b), especially in ALL_AERO simulation (in which atmospheric absorption is high). But, F_{SFC} under clear sky condition (figure 4d) shows that both absorption of shortwave radiation by the atmosphere and reflection at the TOA reduces the solar absorption by the surface uniformly. This also suggests that, in the absence of clouds, the total effect of aerosol radiative forcing is to reduce the incoming solar radiation at the surface. However, in the presence of clouds, the spatial distribution of radiative forcing (figure 4a, b and c) is much more complex with some pockets where the incoming solar radiation is increased. For example, both F_{TOA} and F_{SFC} are increased over the regions such as northern India (north of $\sim 17^{\circ}\text{N}$) where there is strong reduction in cloudiness due to aerosols (figure 5). Thus, the aerosol forcing, which includes reflection and absorption, is considerably augmented by the internal monsoon feedbacks to result in a much more complex spatial distribution than the forcing associated with greenhouse gases which is fairly uniform in space (e.g., Rajendran and Kitoh 2008).

With all three ways of prescribing aerosols, the simulations tend to reduce the total cloud amount over the continental convective regions. The region with maximum reduction in cloudiness (e.g., north of $\sim 17^{\circ}\text{N}$) experiences increased surface solar absorption (figure 4c) (associated with weakened atmospheric solar depletion (figure 4a) due to reduced cloudiness (figure 5)). This suggests that the impact of aerosol forcing on monsoon is highly non-linear because of aerosol-induced changes in cloud-radiation feedback during the monsoon season.

4. Sensitivity of Indian summer monsoon

4.1 Mean monsoon simulation: Model fidelity

The ability of GCMs to realistically simulate the mean Indian summer monsoon rainfall (ISMR) and mean seasonal variation of rainfall over India has been the object of many studies. The Atmospheric Model Intercomparison Project (AMIP) analysis of Gadgil and Sajani (1998) has suggested that those models which realistically simulate the seasonal transition of primary rainbelt over the tropical Indo-Pacific region, are not only more adept at simulating the seasonal mean pattern of ISMR,

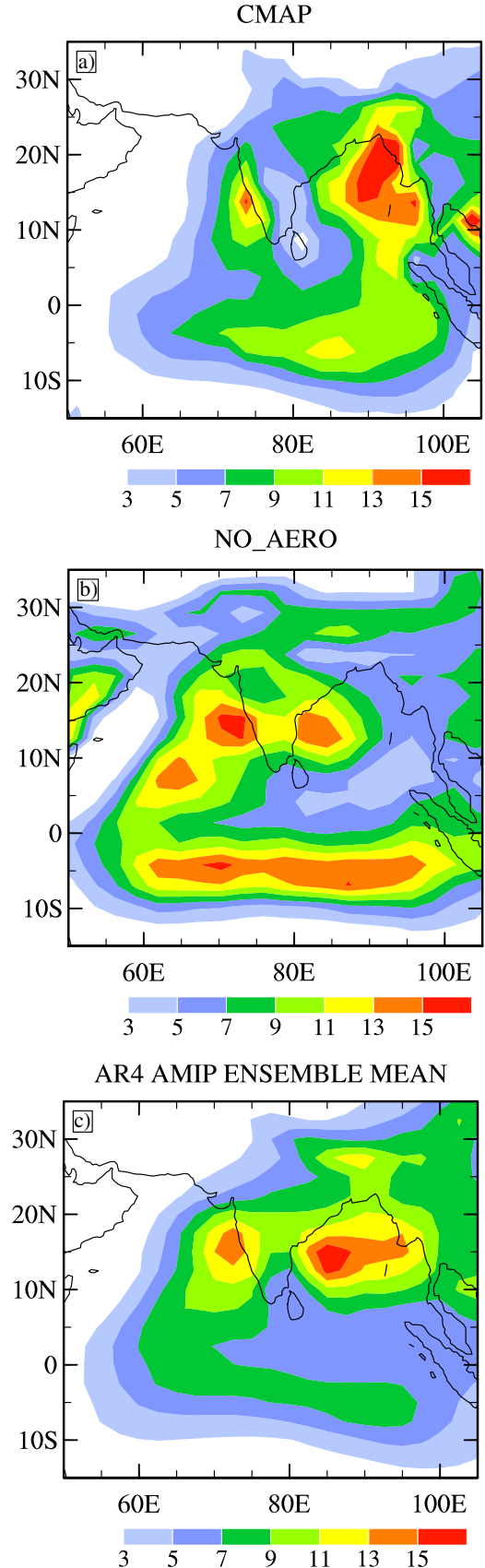


Figure 6. Climatological summer (JJAS) monsoon precipitation over India from (a) CMAP observation, (b) NO_AERO simulation and (c) IPCC AR4 AGCM ensemble mean.

but also are successful in reproducing the year-to-year variation of ISMR associated with major El Niño/La Niña events. Figure 6 shows climatological summer (JJAS) mean precipitation over India from (a) CMAP observation, (b) NO_AERO simulation and (c) IPCC AR4 AGCM multimodel ensemble mean. The observed mean ISMR distribution exhibits multiple favourable positions for mean rainfall maxima. These regions are characterized by organized convection in a sustained manner on seasonal time scales. The primary rainfall maximum (rainbelt) over the monsoon convergence zone coincides with the seasonal mean location of the monsoon trough over India. This extends westwards from northern Bay of Bengal, across the Indo-Gangetic plain. There is a secondary rainbelt over the equatorial Indian Ocean and intense orographic rainfall occurs along the west coast and over the Himalayas. The model captures the essential features such as the extent and location of prominent rainbelts over the Indian region during summer reasonably well. However, the orientation of the simulated rainbelts differ from those in observations. Unlike observation, the simulated primary rainbelt appears to persist around 15°N. The simulated maximum in rainfall over central India occurs slightly south of the observed primary rainbelt. High rainfall is also simulated over orographic regions of the west coast and over the Himalayas. We note that the simulation with CAM3 is comparable to that from the current state-of-the-art AGCMs (figure 6c which shows the IPCC AR4 AGCM multimodel ensemble mean). In view of model's climatological bias, while assessing the aerosol impact, we focus on two regions, viz., (i) the Indian peninsula south of 17°N (as the major rainbelt area) and (ii) the region between 17° and 24°N, where the aerosol concentrations are high and which could have a strong impact on monsoon rainfall, and the high rainfall areas north of it near the Himalayas. The model also overestimates the oceanic rainbelt. We analyse regions north of this rainbelt.

The latitudinal variation of climatological mean precipitation over the Indian region from (a) CMAP observation, (b) NO_AERO simulation and (c) ALL_AERO simulation (figure 7) also shows these features. While the mean seasonal variation of observed rainfall averaged over the Indian sector shows the seasonal migration of rainbelt from the equatorial region in Boreal winter to northern hemisphere in summer, in simulations the monsoon season appears to be longer with nearly semi-permanent rainbelt to the north of the overestimated equatorial oceanic rainbelt. Introduction of aerosol seems to have reduced the intensity of rainfall over model's primary rainbelt (17°–24°N) region (figure 7c).

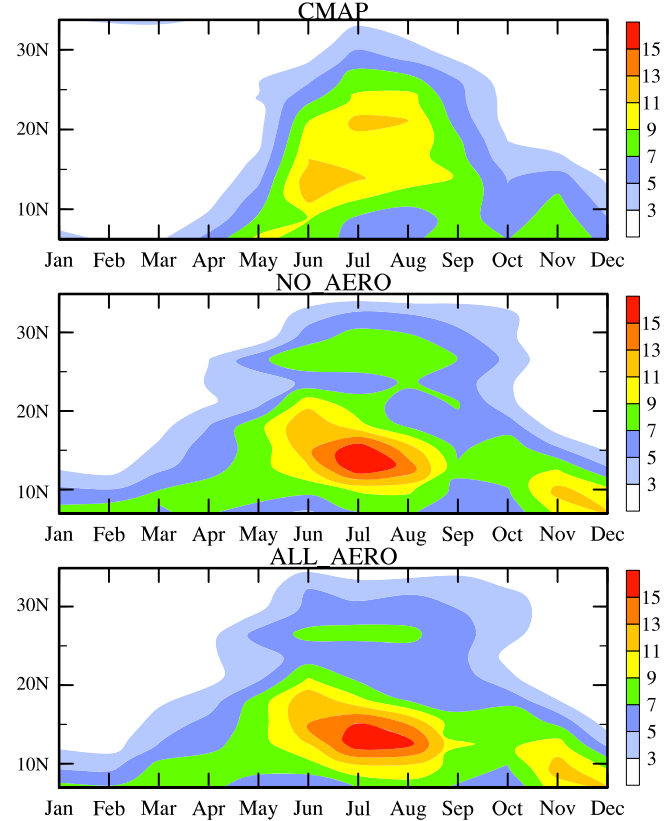


Figure 7. Climatological seasonal cycle of precipitation averaged over Indian longitudes (70°–95°E) from (a) CMAP observation, (b) NO_AERO and (c) ALL_AERO simulations.

4.2 Aerosol impact on Indian summer monsoon

Figure 8 shows mean summer (JJAS) monsoon precipitation from the control simulation (NO_AERO, figure 8a) and the aerosol impact on summer monsoon precipitation given as the differences in JJAS mean precipitation from BKG_AERO, ACE_AERO and ALL_AERO with respect to the control (figure 8b, c, and d). Similarly figure 8 (e and f) shows differences for BC_AERO and SUL_AERO simulations. In NO_AERO (figure 8a), the highest precipitation occurs between 7° and 17°N (with a northwest to southeast tilted rainbelt in the northern margin) along the simulated seasonal ITCZ from northern Africa (centered around 10°N) to east Asia (around 15°N). Over the Indian longitudes, the simulated rainbelt is about 5° south of the observed position of the primary monsoon rainbelt which occurs as a part of the planetary ITCZ in summer (e.g., Gadgil and Sajani 1998). Considerable rainfall also occurs over India between 17° and 30°N. In addition, there is a strong secondary rainbelt over the equatorial Indian Ocean between 7°S and 1°N. The precipitation differences in three aerosol simulations with respect to the control (NO_AERO) summer mean rainfall show strong spatial variations that occur

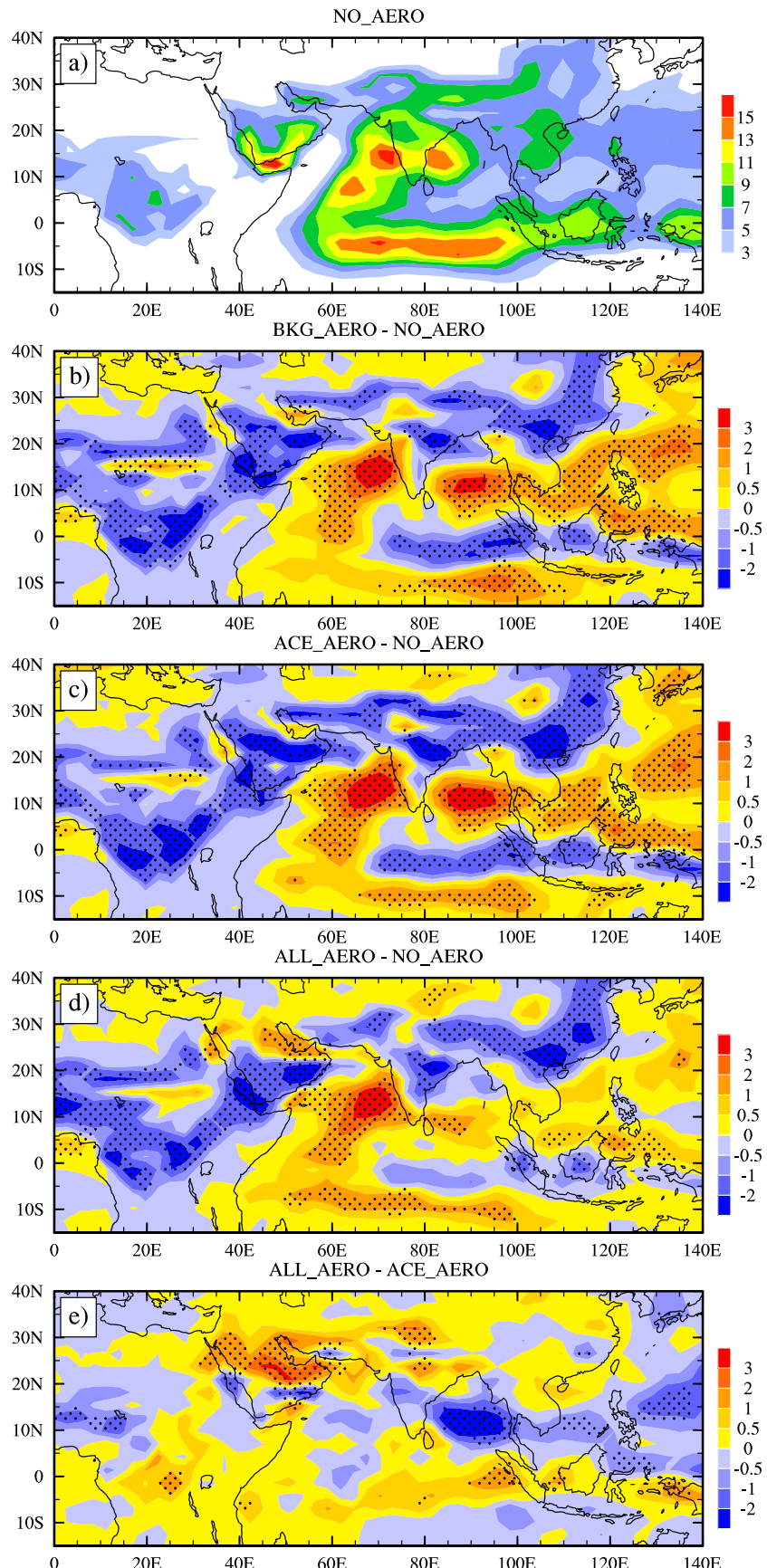


Figure 8. (a) Simulated climatological JJAS mean precipitation (mm day^{-1}) from NO_AERO and JJAS mean precipitation differences (mm day^{-1}) for (b) BKG_AERO, (c) ACE_AERO and (d) ALL_AERO with respect to that from NO_AERO. (e) JJAS mean precipitation difference between ALL_AERO and ACE_AERO. Differences significant at 95% level are stippled.

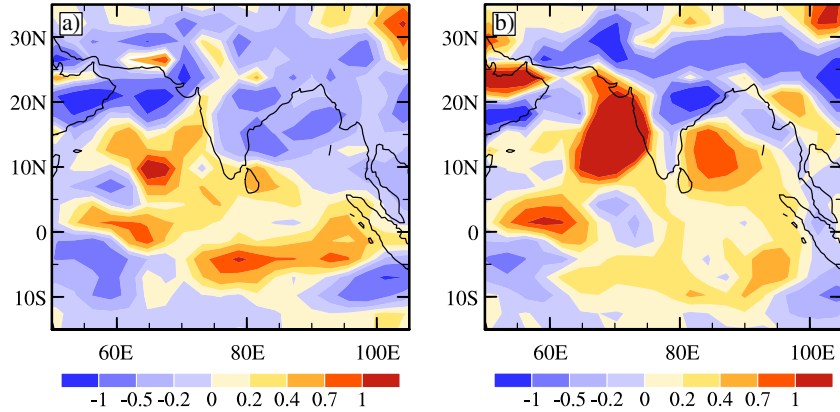


Figure 9. JJAS mean precipitation differences (mm day^{-1}) for (a) BC_AERO and (b) SUL_AERO with respect to that from NO_AERO.

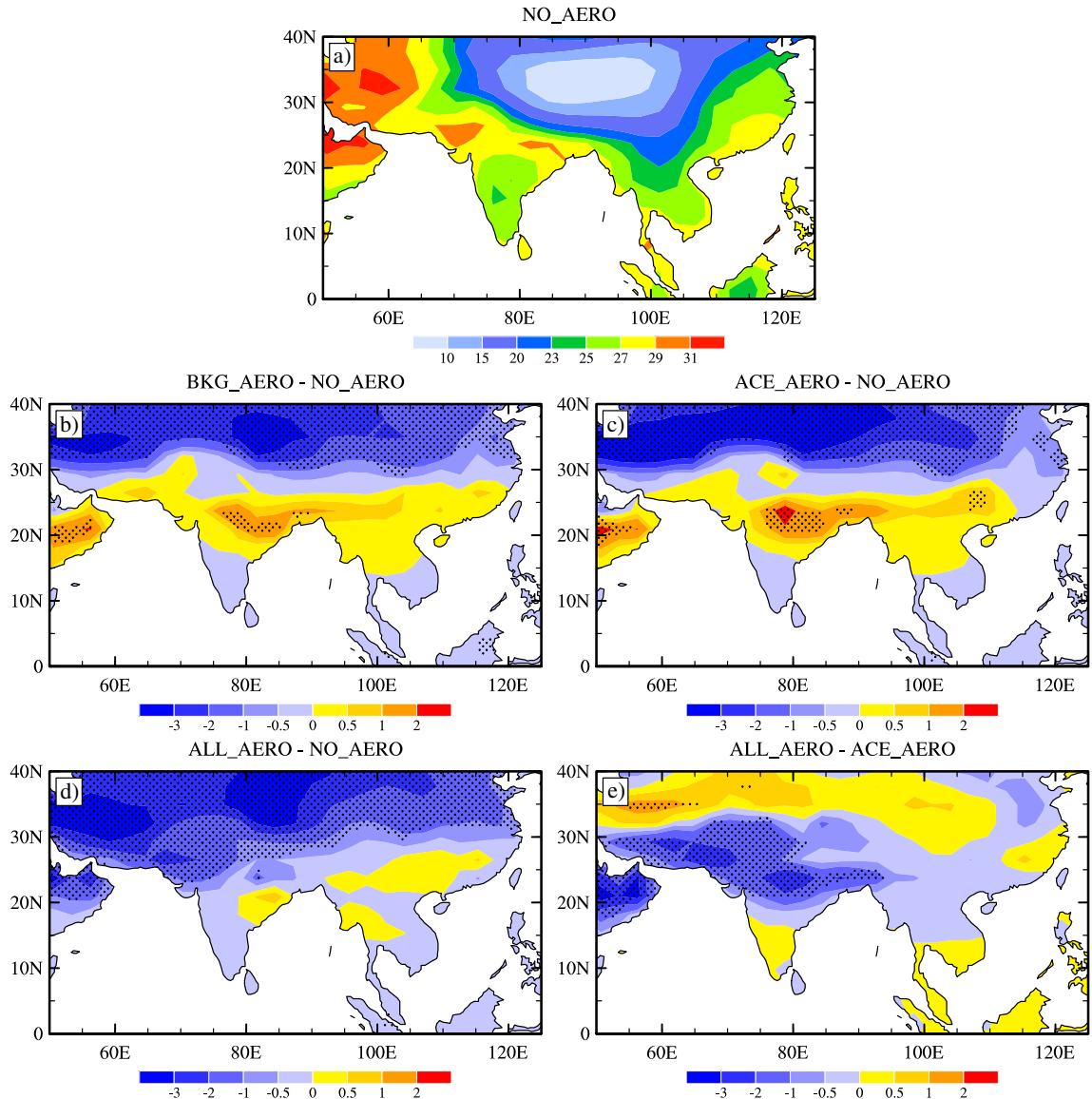


Figure 10. (a) Simulated climatological JJAS mean surface temperature (T_{SFC} in $^{\circ}\text{C}$) from NO_AERO and JJAS mean T_{SFC} differences ($^{\circ}\text{C}$) for (b) BKG_AERO, (c) ACE_AERO and (d) ALL_AERO with respect to NO_AERO. (e) JJAS mean T_{SFC} difference between ALL_AERO and ACE_AERO.

mostly in the ITCZ and marginal regions. Significant differences at 95% level are stippled. Different interactions of radiation and convection with different land conditions mean that the aerosol effects on radiative and latent heating (shown later) is not the same at all locations. In response to aerosol forcing, negative precipitation anomalies occur over continental convective regions and positive anomalies are found over their margins and adjacent oceanic regions in all the aerosol simulations. In spite of quantitative differences, the nature of the impact is qualitatively similar in ALL_AERO as well. Or in other words, the total aerosol and sulphate aerosol induced changes in all the simulations indicate large-scale suppression of summer monsoon precipitation over continental TCZs.

When examined in detail, the differences in BKG_AERO and ACE_AERO (figure 8b and c) show highest reduction in precipitation northward of 17°N, particularly between 17° and 24°N. To the south of this, over the simulated primary monsoon rainbelt region (7°–17°N), there is a strong enhancement in oceanic precipitation on either side of the Indian peninsula and relatively

smaller reduction in peninsular rainfall *vis-a-vis* over the northern region. South of the peninsula, we note an increase in oceanic precipitation. Further south, over part of the secondary rainbelt and just north of it (5°S–3°N) large reduction in rainfall is noticeable. Further southward of this region (12°S–5°S) rainfall increases. Thus, the spatial distribution of rainfall differences clearly suggests a southward shift in the seasonal TCZs over the Indian region due to sulphate aerosol forcing. It also suppresses continental monsoon precipitation. This is consistent with the findings of Williams *et al.* (2001), who found that sulphate aerosols can affect the large-scale atmospheric circulation, particularly in the tropics and cause a southward shift of the ITCZ. This shift was attributed to a reduced inter-hemispheric temperature gradient since reflecting aerosols predominantly cool the Northern Hemisphere. Overall, ALL_AERO (figure 8d) shows qualitatively similar features to those in BKG_AERO and ACE_AERO. However, the impact of absorbing aerosols alone is different on mean precipitation. For example, the difference between ALL_AERO and ACE_AERO JJAS mean precipitation (figure 8e) shows that

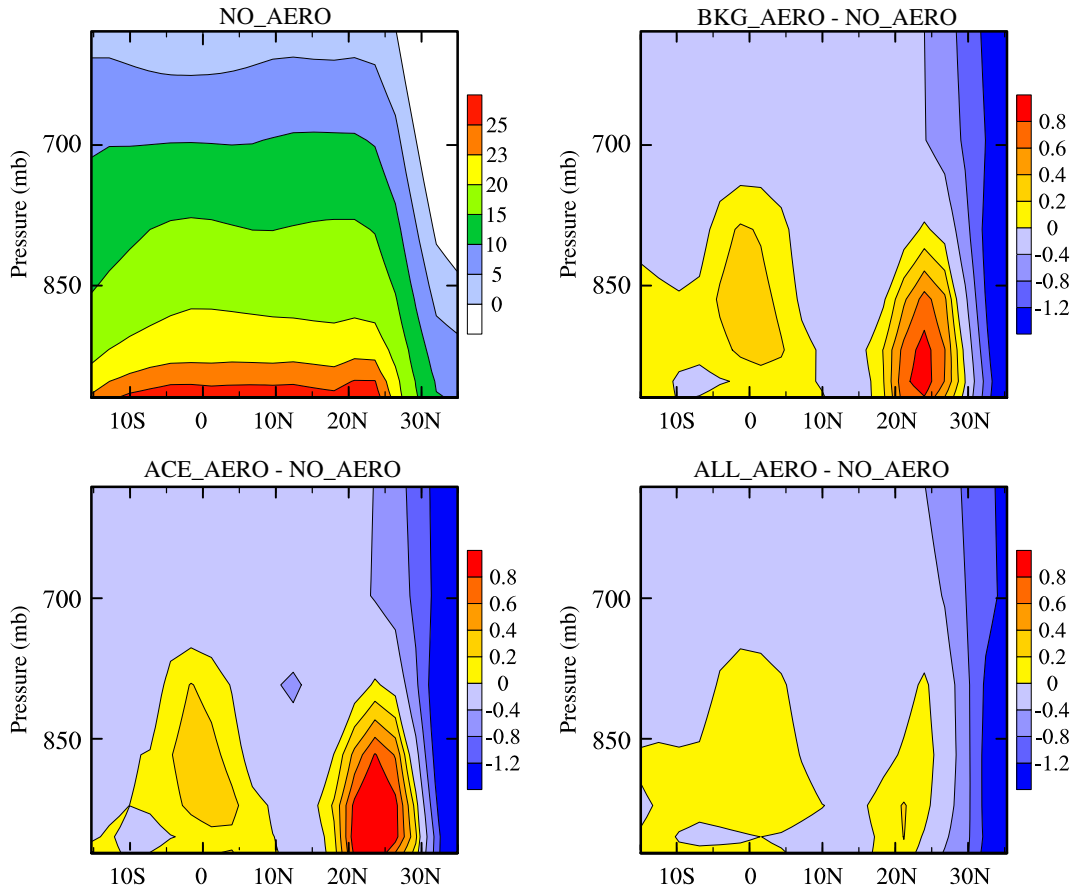


Figure 11. Latitude-pressure section of simulated climatological JJAS mean temperature (°C) averaged over 70°–95°E from NO_AERO (top-left) and JJAS mean temperature differences (°C) for BKG_AERO (top-right), ACE_AERO (bottom-left) and ALL_AERO (bottom-right) with respect to NO_AERO.

absorbing aerosols result in strengthening of major rainbelts with precipitation reduction in marginal areas. Over India, the region between 17° and 24°N where maximum rainfall reduction due to scattering aerosol forcing occurs (as seen in figure 8b, c, and d), the absorbing aerosols cause an enhancement of precipitation (figure 8e). Similarly, the secondary rainbelt over the Indian Ocean also

experiences slight increase in rainfall due to absorbing aerosols. This is also evident in the difference pattern for BC_AERO simulation (figure 9a). However, to isolate absorbing aerosol effect we still use ALL_AERO minus ACE_AERO instead of BC_AERO as it contains only soot (which is absorbing) whose contribution to total aerosol is very less (figure 3) making the BC_AERO AOD

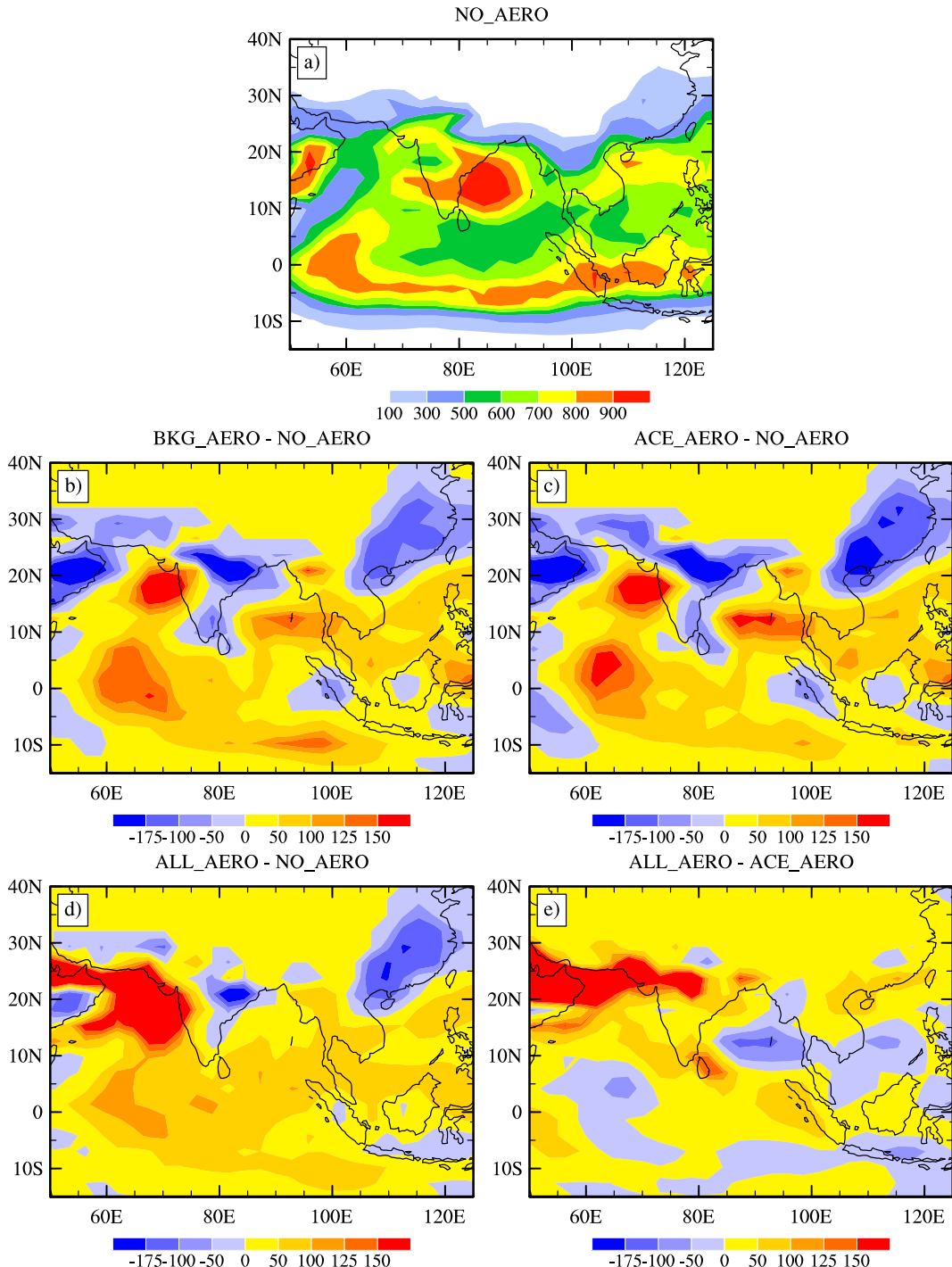


Figure 12. (a) Simulated climatological JJAS mean CAPE from NO_AERO and JJAS mean CAPE differences (J kg^{-1}) for (b) BKG_AERO, (c) ACE_AERO and (d) ALL_AERO with respect to NO_AERO. (e) JJAS mean CAPE difference between ALL_AERO and ACE_AERO.

comparatively very small compared to total AOD in ALL_AERO. For example, dust, which is a dominant component contributing to total aerosol (figure 3), is partially or predominantly absorbing depending on its size and hence is not included in BC_AERO run. Similarly the SUL_AERO simulation (that contains only sulphate) the response of which is found to be closely matching to the other sulphate cases such as ACE_AERO (figure 9b).

Figure 10 shows the summer mean surface temperature (T_{SFC}) over Indian region from NO_AERO (figure 10a) and the differences in T_{SFC} from BKG_AERO, ACE_AERO and ALL_AERO with respect to the control simulation (figure 10b, c, and d). In NO_AERO (figure 10a), the heavy rainfall regions are collocated with large temperature gradient and the TCZs are located to the south of them, with the highest temperatures above 29°C often associated with reduced precipitation. This suggests that the warming/cooling of land surface can be due to changes in surface radiation and also due to feedbacks associated with reduced/enhanced rainfall as well. In this figure, we have shown surface temperature differences only over land region as surface temperature over continental regions is calculated interactively, whereas SST is prescribed over oceans. The effect of absorbing aerosols is to increase the radiative heating of the atmosphere and to reduce the heating of the surface. Therefore, only the atmospheric heating mechanism is effective over oceans. The reduction of incoming solar radiation due to total AOD is apparent from the large-scale surface cooling over most of the continental areas. Examining the differences (figure 10b, c and d) we note that regions with high rainfall located in the control (e.g., figure 8a) i.e., 7°–17°N, aerosol forcing results in cooler land surface. Or in other words, there is surface cooling over the simulated primary rainbelt region. But, the region with maximum precipitation reduction due to aerosols (figure 8b, c, and d), i.e., between 17° and ~24°N, experiences warming of land surface both in BKG_AERO and ACE_AERO. This is the region where the aerosol concentrations are high, and aerosol-induced reduction in total cloudiness (figure 5) and surface solar absorption, F_{SFC} (figure 4c) are very high. Surface temperature changes occur not only due to shortwave changes but can also occur due to cloudiness induced changes in net energy at the surface. Over this region, aerosol simulations show that changes in cloud amount associated with changes in rainfall can strongly limit surface temperature changes. In this case changes in cloudiness closely correspond to changes in net surface energy (not shown). This tendency of surface warming over northern margins of the major rainbelts, which also experience

considerable seasonal mean precipitation are seen over Africa as well (not shown). This suggests that the increased surface solar absorption (figure 4c) due to aerosol induced cloud-radiation feedback could be the major contributing factor for the surface warming. In ALL_AERO, though there exist warm anomalies over this region, they are feeble (corresponding well with the cloudiness changes). Apart from this, most of the continental areas experiences surface cooling due to aerosols. Slightly different response seen in ALL_AERO compared to BKG_AERO and ACE_AERO, can be due to the impact of atmospheric absorption of incoming solar radiation and comparatively smaller changes in F_{SFC} (figure 4c). Absorbing aerosols alone result in reduced surface temperature (figure 10e) over whole of north India concurrent with their tendency to cause weaker rainfall reduction in mean seasonal precipitation compared to that of scattering aerosols, over this region (e.g., ~17°–24°N).

Temperature changes due to aerosols is not confined to the surface alone, instead it extends to the lower tropospheric level up to ~850 hPa. For example, vertical cross sections (latitude-pressure sections) of JJAS mean atmospheric temperature averaged over 70°–95°E from NO_AERO and the differences in corresponding estimates from other simulations with respect to that of the control are shown in figure 11. In NO_AERO, associated with summer monsoon over India, north of equator, there is a northward gradient in temperature especially in the lower troposphere. This positive meridional

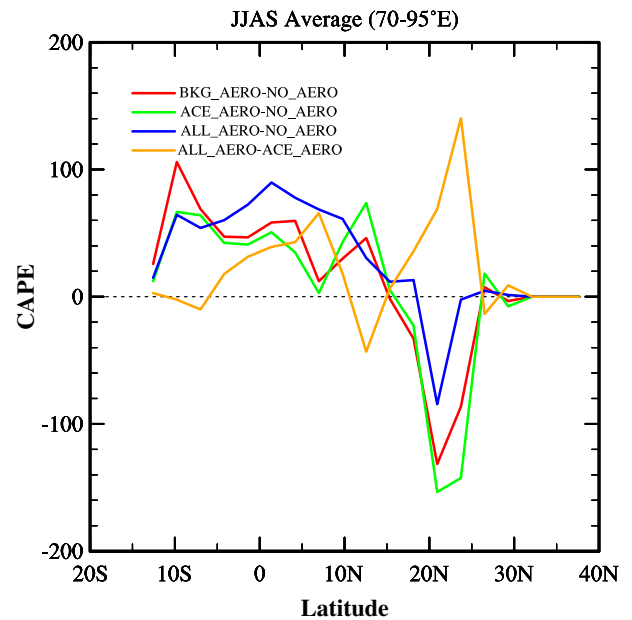


Figure 13. Simulated climatological JJAS mean changes in CAPE (J kg^{-1}) over India (70° – 95° E average) for BKG_AERO, ACE_AERO and ALL_AERO with respect to NO_AERO and CAPE difference between ALL_AERO and ACE_AERO.

gradient in temperature (lower tropospheric land–ocean temperature contrast) is a strong local forcing component for the setting up and maintenance of monsoon apart from the seasonal migration of the planetary ITCZ that occurs in response to the seasonal variation in solar insolation (e.g., Gadgil and Sajani 1998).

In presence of aerosol loading, there is a uniform large-scale cooling of the atmosphere, except for distinct warming over regions north of $\sim 17^{\circ}\text{N}$ (where reduction in continental rainfall was maximum as seen in figure 8) and south of $\sim 9^{\circ}\text{N}$. There is cooling in the region between 9° and 17°N that coincides the simulated mean position of the primary rainbelt (figure 8a). Southward of this region, there is warming over the oceanic region. This suggests that the atmospheric boundary layer over the main rainbelt region in the control simulation ($\sim 9^{\circ}\text{--}17^{\circ}\text{N}$) gets colder and those over the oceanic regions south of this region get warmer. This can weaken the land–ocean surface temperature contrast and the ocean–atmosphere contrast

in the lower troposphere which in turn can weaken landward monsoon circulation and thereby suppress organized convection and precipitation over land. In ALL_AERO, the surface warming over the two latitudinal bands ($17^{\circ}\text{--}24^{\circ}\text{N}$ and south of 9°N) is weakened but still evident in the lower troposphere. This indicates that the impact of total aerosols acts predominantly through scattering, offsetting the impact of absorbing aerosols. This could be due to the fact that the contribution from nonabsorbing aerosols to total AOD is comparable to or larger than that from the absorbing aerosols in ALL_AERO. Various observational studies have shown that there is large uncertainty in the relative amounts of different aerosol types. Randles and Ramaswamy (2008) found that at higher optical depths, enhanced low-level convergence and ascent overcame the stabilizing effects of aerosols and strengthened the monsoon. However, increase in scattering aerosols alone had the opposite effect. Such weakening of the monsoon occurred either with prescribed SSTs (Chung and

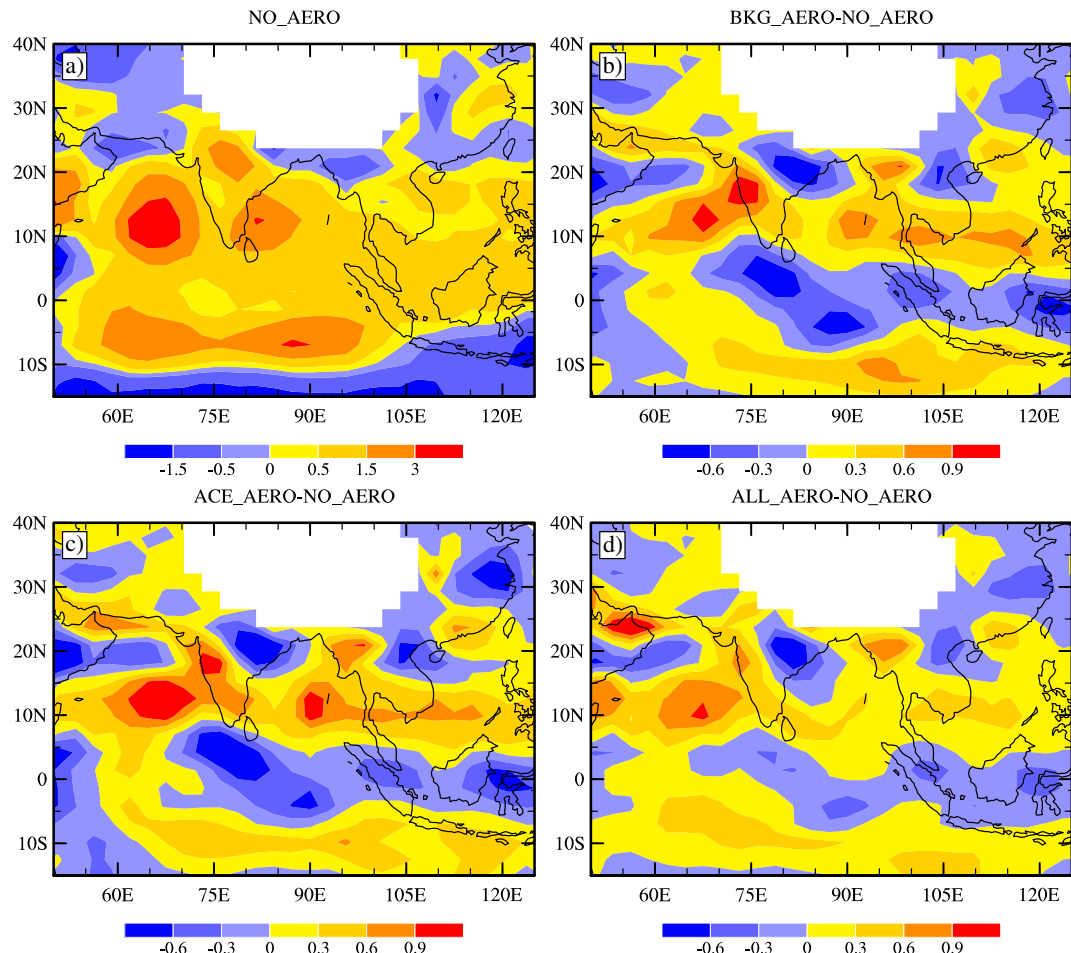


Figure 14. Simulated (a) climatological JJAS mean vertically integrated low level (1000–700 hPa) moisture convergence ($\times 10^{-5}$ kg/kg/s) from NO_AERO and JJAS mean moisture convergence differences for (b) BKG_AERO, (c) ACE_AERO and (d) ALL_AERO with respect to NO_AERO.

Ramanathan 2006; Ramanathan *et al.* 2007) or when prognostic SSTs in a couple model respond to aerosol forcing (Ramanathan *et al.* 2005; Meehl *et al.* 2008). Studies with large contribution from absorbing aerosols to total aerosols, have indicated increase in monsoon precipitation, but accurate partitioning of total aerosols into absorbing and nonabsorbing components, globally or regionally, is yet to be achieved. In GCMs, the absorbing aerosol forcing, carbon in particular, is sometimes underestimated (Sato *et al.* 2003; Koch *et al.* 2009). This could be due to a number of factors including neglect of the internally mixed state

of BC with other aerosols, neglect of biomass burning (about 40% of total BC emission) and BC concentrations that reach their highest values too close to the surface (Ramanathan and Carmichael 2008). But the AOD assimilation in MATCH aerosol transport model gives better confidence in the simulation of different aerosols by this model (Collins *et al.* 2001). The stabilizing effect of reduced tropospheric land–ocean temperature contrast over India is seen from figure 12 which shows JJAS mean convective available potential energy (CAPE) from NO_AERO (figure 12a) and differences in CAPE simulated by the three aerosol

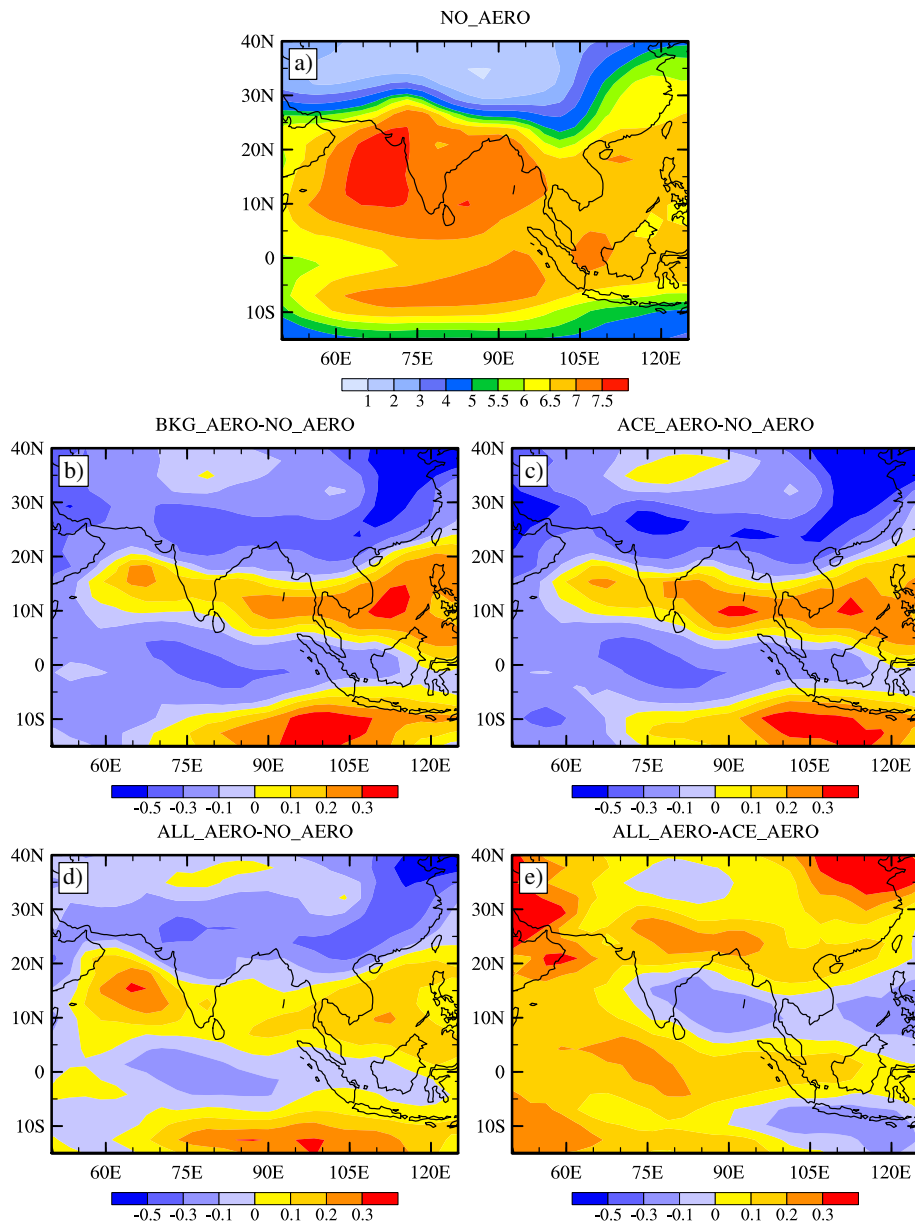


Figure 15. Simulated (a) climatological JJAS mean vertically integrated (1000–700 hPa) specific humidity ($\int q$ in g kg^{-1}) from NO_AERO and JJAS mean $\int q$ differences for (b) BKG_AERO, (c) ACE_AERO and (d) ALL_AERO with respect to NO_AERO. (e) Simulated JJAS mean $\int q$ difference between ALL_AERO and ACE_AERO.

simulations from that of NO_AERO (figure 12b, c, and d). Aerosol induced changes in CAPE averaged over Indian longitudes (70° – 95° N) are shown in figure 13. During summer, mean CAPE is high over unstable regions of ITCZ (figure 8a). Noticeably, due to aerosol radiative forcing CAPE is reduced over Indian monsoon zone (collocating the primary rainbelt over 17° – 24° N), whereas CAPE is increased over the adjacent oceans including the equatorial Indian Ocean (figure 12b, c, and d). This suggests that in response to reduced land–ocean temperature contrast induced by aerosol forcing, the equatorial oceanic atmosphere becomes convectively unstable and Indian monsoon zone atmosphere becomes more stable. Further, it is to be noted that the absorbing aerosols alone exert nearly opposite impact as seen from the difference between CAPE simulated by ALL_AERO and ACE_AERO (figures 12e and 13). One reason is the solar absorption (figure 4a) by absorbing aerosols. This indicates that the increased atmospheric heating due to absorbing aerosols results in increased convective instability and enhancement of precipitation over India. The scattering aerosols do not heat the atmosphere and these are more dominant over the Indian region during summer. This leads to a net suppression of precipitation over India.

4.3 Moisture-advection feedback

The distribution of simulated surface temperature and precipitation changes suggests the role of internal monsoon dynamics and self-amplifying feedback resulting in potentially strong response to perturbations due to the aerosol radiative forcing. Hence, we next analyze plausible dynamic and thermodynamic feedback processes behind the simulated climate response to aerosol forcing. The defining processes fundamental to monsoon dynamics such as the advection of moisture during the monsoon season, convection, precipitation and release of latent heat are important in deciding this climate response.

Figure 14 shows climatological JJAS mean vertically integrated low level (1000–700 hPa) moisture convergence from NO_AERO (figure 14a) and differences in this quantity simulated by BKG_AERO, ACE_AERO and ALL_AERO simulations from that by NO_AERO (figure 14b, c, and d). Figure 15 is similar to figure 14 but for vertically integrated low level specific humidity. NO_AERO simulation shows strong moisture convergence and low level specific humidity over the Indian region associated with Indian summer monsoon. Peaks of convergence and specific humidity coincides with

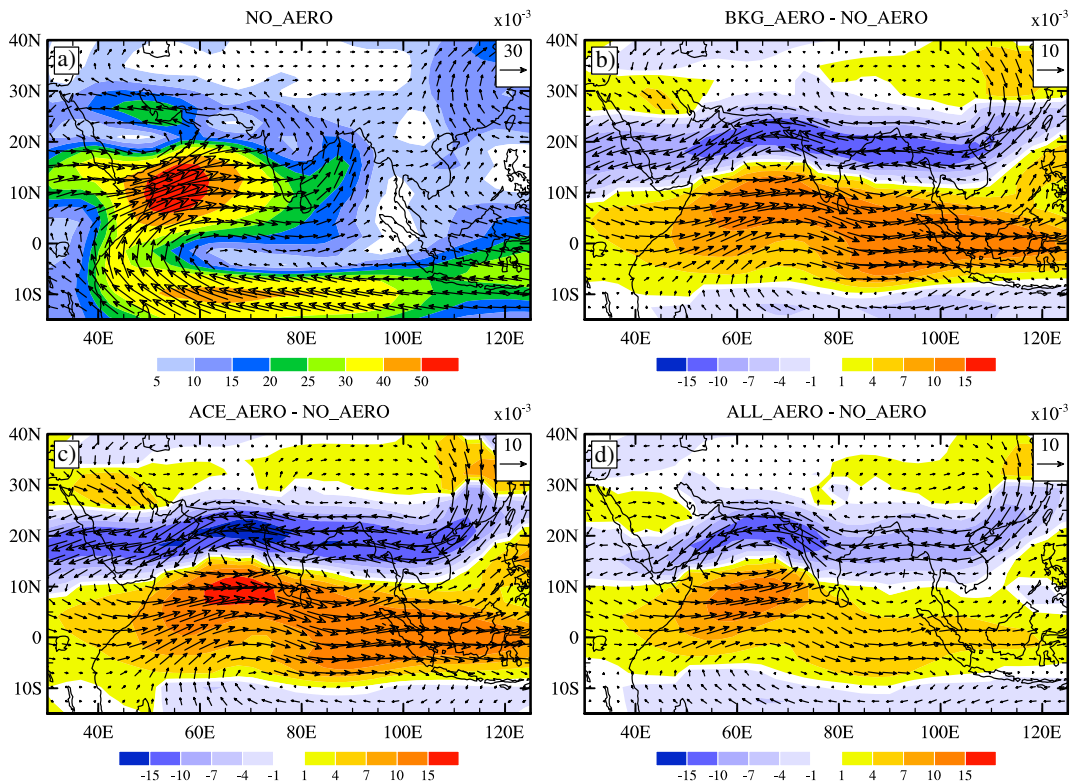


Figure 16. Simulated (a) climatological JJAS mean moisture transport (in vectors with magnitude $\times 10^{-3}$ kg/kg m s^{-1} in shading) from NO_AERO and JJAS mean moisture transport difference (vectors and magnitudes in shading) for (b) BKG_AERO, (c) ACE_AERO and (d) ALL_AERO with respect to NO_AERO.

the major seasonal rainbelts over India and equatorial Indian Ocean. Over northern parts of the continental rainfall regions, the moisture convergence and specific humidity in lower troposphere are also reduced in all the aerosol simulations. This is mainly associated with reduced meridional moisture transport into the region (figure 16 which is similar to figure 14, but for low level moisture transport). It can be seen that meridional transport of moist air from warm equatorial ocean penetrates only up to about 17°N in eastern India (with a northwestward tilt) with the maxima located over Arabian Sea and Bay of Bengal on either side of the southern peninsular region (figure 16a). North of this region, we find that either the moisture transport from the southern seas is very small or weak advection of subtropical air into the region occurs. In response to aerosol forcing, low-level moisture convergence (figure 14b, c, and d), specific humidity (figure 15b, c, and d) and meridional moisture transport (figure 16b, c, and d) are reduced/reversed over continental and oceanic regions where the rainfall is lower due to aerosol forcing (figure 8b, c, and d).

Correspondingly, CAPE, convection and clouds (cloud cover is a function of relative humidity in the model) are also reduced over these regions. In response to these dynamical changes, the release of latent heat (shown in figure 17 which is similar to figure 14b, c, and d, but for latent heat flux) over India is also considerably reduced in all aerosol simulations. If monsoon winds get weaker, condensation and therefore latent heat release through precipitation are reduced. Thus, the strongest impact is seen in latent heating, where the reduction is widespread over monsoonal land regions. In conjunction, increased convection over adjacent ocean is associated with increased latent heat release. During a normal monsoon season, latent heat release dominates the atmospheric heat content. In response to latent heat release, thermal energy is transported out of the region through large-scale advection and synoptic processes. The main dynamical driver of the monsoon is therefore the positive moisture-advection feedback. But, in model, the reduction in precipitation over India in response to aerosol forcing appears to be largely due to a negative moisture-advection feedback. The absorbing aerosols alone result in nearly the opposite climate response (e.g., figure 15e for ALL_AERO-ACE_AERO), but is not strong enough to overcome the effect of scattering aerosols.

In our study, in the presence of aerosols, the solar radiation absorption at the surface is decreased (figure 4) and cloudiness is reduced. The land surface and lower tropospheric temperatures also show a reduction. This reduction in temperature in

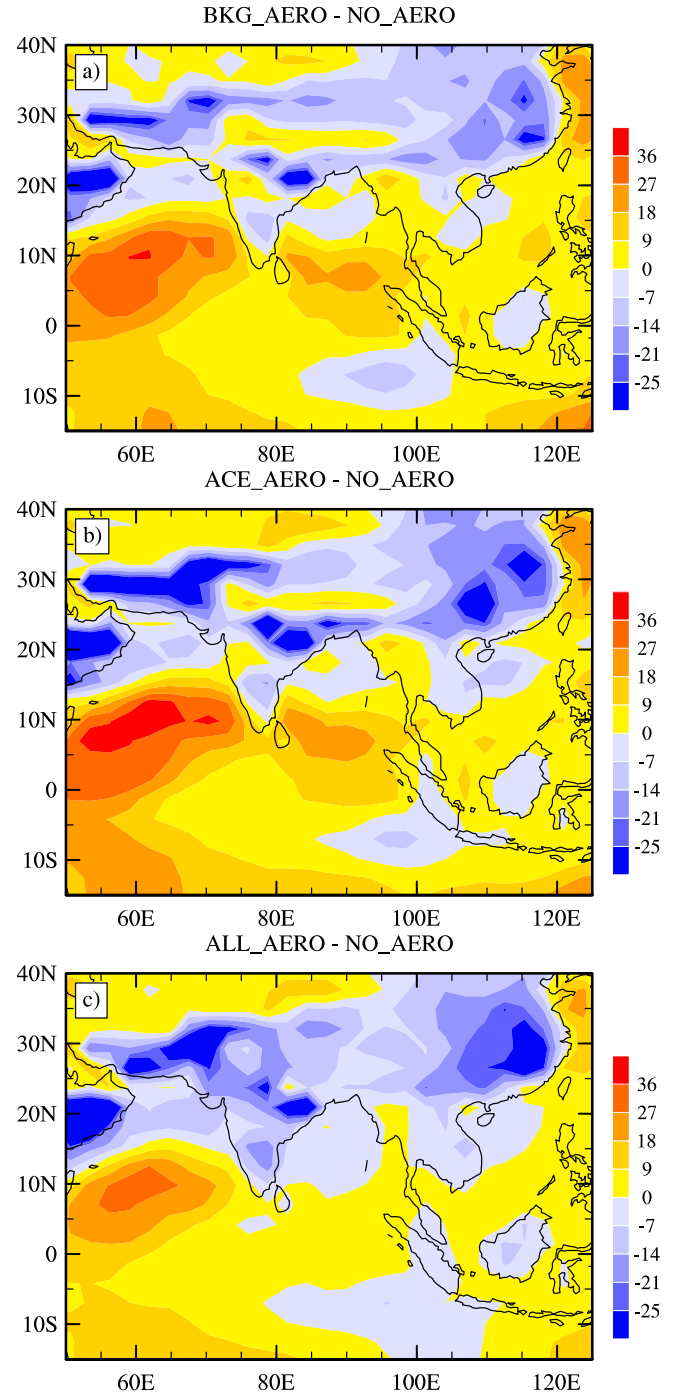


Figure 17. Simulated climatological JJAS mean latent heating (positive into the atmosphere) differences (in W m^{-2}) for (a) BKG_AERO, (b) ACE_AERO and (c) ALL_AERO with respect to NO_AERO.

conjunction with simultaneous increase in the temperature of marine atmosphere in the south (figure 11) reduces the lower land-ocean temperature contrast in the lower troposphere and thereby weakens moisture transport into the monsoon zone, i.e., the advection of moisture towards land (figure 16). This decreases organized convection, clouds, precipitation (figure 8) and the latent

heat release (figure 17). The decrease in release of latent heat from precipitation over land further reduces the temperature difference between land and ocean. This in turn weakens winds from ocean to land, decreasing the landward advection of moisture. The reduced moisture advection in turn leads to lower precipitation and latent heat release. On seasonal time scale, this continued negative feedback results in suppression of monsoon precipitation over India in response to aerosol direct radiative forcing. It is worth noting that changes in the overall intensity of the hydrological cycle are not only controlled by the availability of atmospheric moisture, but also by the availability of energy at the surface (Boer 1993). In our model simulations, aerosol effects are large enough to reduce the availability of total radiative energy at the surface, so that the non-radiative fluxes decline and the global water cycle weakens, i.e., aerosol direct radiative forcing essentially weakens the monsoon hydrological cycle. In summary, in this study,

with all the prescribed aerosol experiments, a weakening of Indian monsoon is obtained in response to a near-realistic total aerosol forcing that causes negative moisture-advection feedback and increased atmospheric stability.

4.4 Impact of regional aerosols

It is to be noted that the spatial distribution of aerosol climate impact is highly sensitive to the way in which aerosol is prescribed. For example, there exist marked differences in seasonal mean precipitation and T_{SFC} between ACE_AERO and BKG_AERO simulations (figure 18a and b) both having scattering aerosols with quantitative differences only over the tropical Indian region (represented by the rectangular box. Significant differences at 90% level are stippled). It can be seen that although the aerosol impact on monsoon precipitation and surface temperature are qualitatively

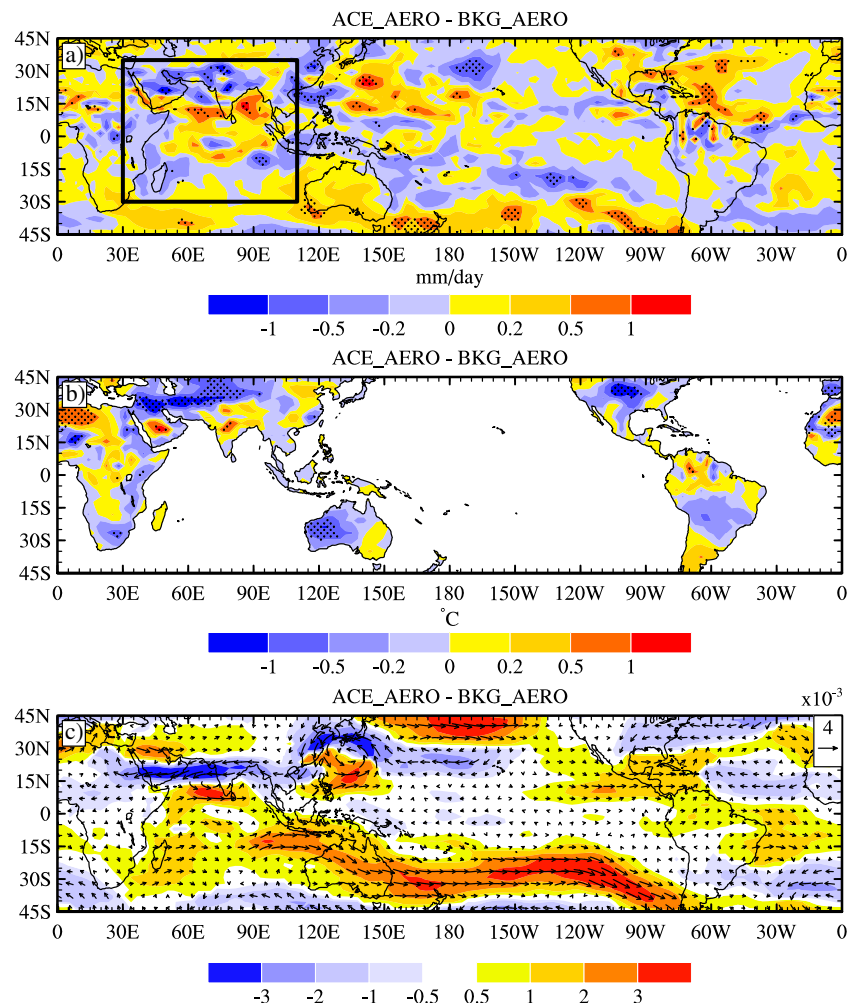


Figure 18. Simulated climatological JJAS mean differences in (a) precipitation (top), (b) T_{SFC} (middle) and (c) moisture transport (vectors and magnitude $\times 10^{-3} \text{ kg/kg m s}^{-1}$ in shading, bottom panel) between ACE_AERO and BKG_AERO.

similar in both simulations (figures 8 and 10), there are noticeable quantitative differences not only over Indian region (where AODs are different) but over remote regions as well. Quantitative changes in AODs over the Indian region result in further reduction of precipitation, significant at 90% level, over continental TCZs of north Africa, India, east Asia and maritime continents of west Pacific, and enhancement of precipitation over marginal areas and adjacent oceans. Similarly T_{SFC} changes in BKG_AERO (figure 10b) are also strengthened in ACE_AERO. Thus, the aerosol-climate impact seen in BKG_AERO (figures 8b, and 10b) is reinforced by prescribing real AODs over Indian monsoon region. This shows that the local and remote impacts of regional aerosols on simulated climate are large and warrants the need to estimate accurate aerosol properties in strategic regions of importance.

Further, moisture transport induced by aerosol radiative forcing over the aerosol loading region modifies that of the outside region (figure 18c). These circulation changes also indicate that the strengthening of aerosol impact in ACE_AERO is not limited to the region of loading, but extends to the whole of tropical Asia Pacific. The regions where precipitation is decreased (increased) experience reduction/reversal (reinforcement) of moisture transport. This implies that the aerosol properties and spatial distributions over a region may make the hydrological cycle more complicated over the broader area. Hence, it is reasonable to anticipate that aerosols may contribute to climate change regionally through radiative forcing-climate feedbacks, and globally through teleconnection.

5. Conclusions

In spite of many studies, aerosol forcing remains a dominant uncertainty in climate studies. While the previous studies indicate plausible but different scenarios of aerosol impacts, they suggest that the impact of aerosol direct radiative forcing on Indian monsoon water cycle dynamics is extremely complex and is strongly dependent on the model, aerosol distribution and characteristics specified in the model, modelling strategy employed as well as on spatial and temporal scales.

In this study we analyzed

- the aerosol direct radiative forcing impact on mean Indian summer monsoon when a combination of quasi-realistic mean annual cycles of scattering and absorbing aerosols derived from an aerosol transport model constrained with satellite observed Aerosol Optical Depth (AOD) is prescribed,

- the dominant feedback mechanism behind the simulated impact of all-aerosol direct radiative forcing on monsoon, and
- the relative impacts of absorbing and scattering aerosols on mean Indian summer monsoon using the Community Climate Model Version 3 (CAM3) that has a comprehensive treatment of the aerosol-radiation interaction.

This AGCM has been used to perform climate simulations with three different representations of aerosol direct radiative forcing due to the total, scattering aerosols and black carbon aerosols. We have also conducted experiments without any aerosol forcing.

Aerosol direct impact due to scattering aerosols is found to cause significant reduction in summer monsoon precipitation over India with a tendency for southward shift of Tropical Convergence Zones (TCZs) over the Indian region. Aerosol forcing reduces surface solar absorption over the primary rainbelt region of India and reduces the surface and lower tropospheric temperatures over the primary continental rainbelt. This cooling in conjunction with simultaneous warming of marine atmosphere of warm ocean in the south reduces the lower tropospheric land-ocean temperature contrast and weakens the advection of moisture into the monsoon zone. This increases atmospheric convective stability, and decreases convection, clouds, precipitation and associated latent heating. The decrease in the release of latent heat from precipitation over land further reduces the land-ocean temperature contrast, and weakens landward advection of moisture. This in turn weakens the monsoon overturning circulation and results in suppressed precipitation and reduced latent heat release. Thus, although details of monsoon sensitivity are complicated, our analysis reveals a defining negative moisture-advection feedback that dominates the seasonal heat balance and acts as an internal damping mechanism spinning down the regional hydrological cycle and leading to significant circulation changes in response to external radiative forcing perturbations. These results indicate that in addition to the surface shortwave reduction, dynamic circulation induced by aerosol forcing is important for understanding climate change over the region.

When the aerosol loading that contains both absorbing and scattering aerosols, is prescribed from three-dimensional monthly distribution of tropospheric aerosols derived from an Atmospheric Transport Model (MATCH), dust and black carbon aerosols cause significant atmospheric heating over the monsoon region. But, the resultant impact on monsoon still shows the dominance of the direct radiative forcing of scattering aerosols acting through negative moisture-advection feedback

to result in significant decrease of summer monsoon precipitation. It is seen that the scattering aerosol-induced weakening of meridional lower tropospheric temperature gradient (leading to weaker summer monsoon rainfall) more than offsets the increase in summer-time rainfall resulting from the atmospheric heating effect of absorbing aerosols, leading to a net decrease of summer monsoon rainfall.

We have also carried out climate simulations with globally constant AODs and also with the constant AODs over the extended Indian region replaced by realistic AODs. Regional aerosol radiative forcing perturbations over the Indian region is found to have impact not only over the region of loading but over remote tropical regions as well. This warrants the need to prescribe realistic aerosol properties in strategic regions such as India in order to accurately assess the aerosol impact.

Acknowledgements

The authors are grateful to Prof. J Srinivasan for scientific inputs throughout the study and critical comments on the first version of the manuscript. SS and KR acknowledge the support from Dr Gangan Prathap. The simulations were carried out in C-MMACS HPC. This work was supported by the project R-8-113 under CSIR-EMPOWER Scheme. RSN thanks INCOIS and MoES for their support.

References

Boer G J 1993 Climate change and the regulation of the surface moisture and energy budgets; *Clim. Dyn.* **8** 225–239.

Bollasina M, Nigam S and Lau K M 2008 Absorbing aerosols and summer monsoon evolution over South Asia: An observational portrayal; *J. Climate* **21** 3221–3239.

Briegleb B P 1992 Delta-Eddington approximation for solar radiation in the NCAR Community Climate Model; *J. Geophys. Res.* **97** 7603–7612.

Cess R D 1985 Nuclear war: Illustrative effects of atmospheric smoke and dust upon solar radiation; *Clim. Change* **7** 237–251.

Chakraborty A, Satheesh S K, Nanjundiah R S and Srinivasan J 2004 Impact of absorbing aerosols on the simulation of climate over the Indian region in an atmospheric general circulation model; *Ann. Geophys.* **22** 1421–1434.

Chung C E and Ramanathan V 2006 Weakening of the north Indian SST gradients and the monsoon rainfall in India and the Sahel; *J. Climate* **19** 2036–2045.

Chung C E, Ramanathan V and Kiehl J T 2002 Effects of the south Asian absorbing haze on the northeast monsoon and surface-air heat exchange; *J. Climate* **15** 2462–2476.

Coakley J A, Cess R D and Yurevich F B 1983 The effect of tropospheric aerosols on the Earth's radiation budget: A parameterization for climate models; *J. Atmos. Sci.* **40** 116–138.

Collier J C and Zhang J 2009 Aerosol direct forcing of the summer Indian monsoon as simulated by the NCAR CAM3; *Clim. Dyn.* **32** 313–332.

Collins W D 1998 A global signature of enhanced short-wave absorption by clouds; *J. Geophys. Res.* **103** 31,669–31,679.

Collins W D, Rasch P J, Eaton B E, Khattatov B, Lamarque J-F and Zender C S 2001 Simulating aerosols using a chemical transport model with assimilation of satellite aerosol retrievals: Methodology for INDOEX; *J. Geophys. Res.* **106** 7313–7336.

Collins W D, Bitz C M, Blackmon M L, Bonan G B, Bretherton C S, Carton J A, Chang P, Doney S C, Hack J J, Henderson T B, Kiehl J T, Large W G, McKenna D S, Santer B D, Santer B D and Smith R D 2006a The Community Climate System Model Version 3 (CCSM3); *J. Climate* **19** 2122–2143.

Collins W D, Rasch P J, Boville B A, Hack J J, McCaa J R, Williamson D L and Briegleb B P 2006b The formulation and atmospheric simulation of the Community Atmospheric Model Version 3 (CAM3); *J. Climate* **19** 2144–2161.

Forster P, Ramaswamy V and Co-authors 2007 Changes in atmospheric constituents and in radiative forcing; In: Climate Change 2007: The Physical Science Basis. Contribution of Working Group I to the Fourth Assessment Report of the Intergovernmental Panel on Climate Change (eds) Solomon S and Co-authors (Cambridge, United Kingdom and New York, NY, USA: Cambridge University Press).

Gadgil S and Sajani S 1998 Monsoon precipitation in the AMIP runs; *Clim. Dyn.* **14** 659–689.

Haywood J M, Roberts D L, Slingo A and Edwards J M and Shine K P 1997 General circulation model calculations of the direct radiative forcing by anthropogenic sulfate and fossil-fuel soot aerosol; *J. Climate* **19** 1562–1577.

Hess M, Koepke P and Schult I 1998 Optical properties of aerosols and clouds: The software package OPAC; *Bull. Am. Meteor. Soc.* **79** 831–844.

Joseph J H, Wiscombe W J and Weinman J A 1976 The delta-Eddington approximation for radiative flux transfer; *J. Atmos. Sci.* **33** 2452–2459.

Kalnay E, Kanamitsu M, Kistler R, Collins W and co-authors 1996 The NCEP/NCAR 40-year reanalysis project; *Bull. Am. Meteor. Soc.* **77** 437–471.

Kiehl J T and Briegleb B P 1993 The relative roles of sulphate aerosols and greenhouse gases in climate forcing; *Science* **260** 311–314.

Koch D and Co-authors 2009 Evaluation of black carbon estimations in global aerosol models; *Atmos. Chem. Phys.* **9**(22) 9001–9026.

Lau K M, Kim M K and Kim K M 2006 Asian monsoon anomalies induced by aerosol direct effects; *Clim. Dyn.* **26** 855–864, doi: [10.1007/s00382-006-0114-z](https://doi.org/10.1007/s00382-006-0114-z).

Meehl G A, Arblaster J M and Collins W D 2008 Effects of black carbon aerosols on the Indian monsoon; *J. Climate* **21**(12) 2869–2882.

Menon S, Hansen J, Nazarenko L and Luo Y 2002 Climate effects of black carbon aerosols in China and India; *Science* **297** 2250–2253.

Mitchell J F B, Davis R A, Ingram W J and Senior C A 1995 On surface temperature, greenhouse gases, and aerosols: Models and observations; *J. Climate* **8** 2364–2386.

Moorthy K K, Nair P R and Satheesh S K 1998 On the climatology of aerosol optical depths. Global Change Studies; ISRO:GBP(GSC-02-98), pp. 45–66.

Rajendran K and Kitoh A 2008 Indian summer monsoon in future climate projection by a super high resolution global model; *Curr. Sci.* **95**(11) 1560–1569.

Ramanathan V, Chung C, Kim D, Betge T, Buja L, Kiehl J T, Washington W M, Fu Q, Sikka D R and Wild M 2005 Atmospheric brown clouds: Impacts on South Asian climate and hydrological cycle; *Proc. Nat. Acad. Sci. USA* **102** 5326–5333, doi: [10.1073/pnas.0500656102](https://doi.org/10.1073/pnas.0500656102).

Ramanathan V, Ramana M V, Roberts G, Kim D, Corrigan C, Chung C and Winker D 2007 Warming trends in Asia amplified by brown cloud solar absorption; *Nature* **448** 575–578.

Ramanathan V and Carmichael G 2008 Global and regional climate changes due to black carbon; *Nature Geosci.* **1** 221–227.

Randles C A and Ramaswamy V 2008 Absorbing aerosols over Asia: A geophysical fluid dynamics laboratory general circulation model sensitivity study of model response to aerosol optical depth and aerosol absorption; *J. Geophys. Res.* **113** D21203, doi: [10.1029/2008JD010140](https://doi.org/10.1029/2008JD010140).

Rasch P J, Mahowald N M and Eaton B E 1997 Representations of transport, convection, and the hydrologic cycle in chemical transport models: Implications for the modeling of short-lived and soluble species; *J. Geophys. Res.* **102** 28,127–28,138.

Rayner N A, Parker D E, Horton E B, Folland C K, Alexander L V, Rowell D P, Kent E C and Kaplan A 2003 Global analyses of SST, sea ice and night marine air temperature since the late nineteenth century; *J. Geophys. Res.* **108**, doi: [10.1029/2002JD002670](https://doi.org/10.1029/2002JD002670).

Roeckner E L, Bengtsson L, Feichter J, Lelieveld J and Rodhe H 1999 Transient climate change simulations with a coupled atmosphere-ocean GCM including the tropospheric sulfur cycle; *J. Climate* **12** 3004–3031.

Sato M, Hansen J, Koch D, Lacis A, Ruedy R, Dubovik O, Holben B, Chin M and Novakov T 2003 Global atmospheric black carbon inferred from AERONET; *Proc. Nat. Acad. Sci. USA* **100**(11) 6319–6324.

Streets D G and Waldhoff S T 2000 Present and future emissions of air pollutants in China: SO₂, NO_x, and CO; *Atmos. Environ.* **34** 363–374.

Wang C, Kim D, Ekman A M L, Barth M C and Rasch P J 2009 Impact of anthropogenic aerosols on Indian summer monsoon; *Geophys. Res. Lett.* **36** L21704, doi: [10.1029/2009GL040114](https://doi.org/10.1029/2009GL040114).

Williams K D, Jones A, Roberts D L, Senior C A and Woodage M J 2001 The response of the climate system to the indirect effects of anthropogenic sulfate aerosol; *Clim. Dyn.* **17** 845–856.

Xie P and Arkin P A 1997 Global precipitation: A 17-year monthly analysis based on gauge observations, satellite estimates, and numerical model outputs; *Bull. Am. Meteor. Soc.* **78** 2539–2558.

Zhang G J and McFarlane N A 1995 Sensitivity of climate simulations to the parameterization of cumulus convection in the Canadian Climate Centre general circulation model; *Atmos. Ocean* **33** 407–446.

Zhang H, Wang Z, Pinwen G and Wang Z 2009 A modeling study of the effects of direct radiative forcing due to carbonaceous aerosol on the climate in east Asia; *Adv. Atmos. Sci.* **26** 57–66.

MS received 16 May 2011; revised 4 November 2011; accepted 10 March 2012